CARDIAC MTSS1 DOWNREGULATION PROTECTS AGAINST DILATED CARDIOMYOPATHY IN A SEX-SPECIFIC MANNER

Dongwook Christian Choe

A DISSERTATION
In
Cell and Molecular Biology
Presented to the Faculties of The University of Pennsylvania
In
Partial Fulfillment of the Requirements for the
Degree of Doctorate of Philosophy
2024

Supervisors of Dissertation:

Kiran Musunuru, M.D., Ph.D.
Professor of Medicine (Cardiovascular Medicine)

Thomas P. Cappola, M.D.
Professor of Medicine

Graduate Group Chairperson:

Dan Kessler, Ph.D.
Chair, Cell and Molecular Biology Graduate Group

Dissertation Committee:

Chair: Zoltan P. Arany, M.D., Ph.D.
Professor of Cardiology

Sharlene M. Day, M.D.
Associate Professor of Medicine

Rajan Jain, M.D.
Associate Professor of Medicine (Cardiovascular Medicine)

Benjamin L. Prosser, Ph.D.
Associate Professor of Physiology

Acknowledgements

This thesis would not have been possible without the guidance and support of Dr. Kiran Musunuru. His support of high-risk science made this project possible and his insights drove much of the work. I would also like to thank Dr. Thomas Cappola. Not only did he effectively act as a second mentor, his enthusiasm and encouragement were appreciated over the course of this thesis. My thesis committee was incredibly helpful both inside and outside of regular meetings.

I would like to thank Professor Xiao Wang, whose advice on everything from mouse handling to iPSC care for the past seven years was deeply appreciated. Dr. Nataliya Petrenko's work on patch-clamping cardiomyocytes and her skill at electrophysiology are as impressive as the size of her heart and the Ukrainian breads she bakes. Jeffrey Brandimarto's help with genotyping, immunohistochemistry, and general protein work made much of the scientific work dramatically easier. Dr. Alexandra Chadwick showed me the ropes when I first joined the lab. Professor Chris McDermott-Roe and Dr. Jane Lv helped teach work concerning iPSCs.

Mike Morley and Yifan Yang were instrumental for the bioinformatics presented in this thesis. I must thank the members of the CVI Stem Cell Core, the Transgenic Mouse Genome Editing Core, Mouse Physiology Core, and the Histology Core for creating and editing iPSCs, creating mouse lines, conducting echocardiography, and creating excellent embryonic sections.

Finally, I would like to thank my family; their support has been invaluable in too many ways to list for 32 years and counting. And I would like to thank my friends for their support inside the lab and out. It has been an interesting experience; we'll see what's ahead.

Abstract

CARDIAC MTSS1 DOWNREGULATION PROTECTS AGAINST DILATED CARDIOMYOPATHY IN A SEX-SPECIFIC MANNER

Dongwook Choe

Kiran Musunuru

Thomas P. Cappola

Enhancer variants that reduce the expression of MTSS1 in the human left ventricle have been associated with cardioprotective traits in genome-wide association studies. However, the effect of MTSS1 downregulation on the development of heart disease had not been studied in cell or animal models and warranted further investigation. In this study, we evaluated whether cardiac MTSS1 downregulation could be protective against dilated cardiomyopathy. To do this, we 1) assessed the associations of *MTSS1* enhancer variants with a variety of cardiac structural and functional traits, as well as phenome-wide traits, in the UK Biobank cohort, both in the general cohort and stratified by sex. We also 2) used a mouse model of dilated cardiomyopathy [Tg(Myh6-Tpm1*D230N)HJcf] to test the effect of heterozygous knockout of the mouse *Mtss1* ortholog on cardiac structural and functional traits separately in female mice and male mice. Finally, we 3) knocked out *MTSS1* in two induced pluripotent stem cell-cardiomyocyte models of dilated cardiomyopathy [TNNT2 R173W] [TPM1 D230N] and measured their spontaneous beating rate response to isoproterenol induction.

In summation, my thesis provides 1) evidence that cardiac *MTSS1* downregulation in the female sex protects against dilated cardiomyopathy and 2) evidence that cardiac *MTSS1* downregulation in the male sex has no effect against dilated cardiomyopathy.

TABLE OF CONTENTS

ACKNOWLEDGEMENTS ii
ABSTRACT iv
LIST OF TABLES vi
LIST OF FIGURES vii
CHAPTER 1: INTRODUCTION 1
CHAPTER 2: METHODS 19
CHAPTER 3: BIOINFORMATICS 32
CHAPTER 4: MURINE STUDIES 41
CHAPTER 5: iPSC-CARDIOMYOCYTES 56
CHAPTER 6: DISCUSSION 60
BIBLIOGRAPHY: 64

LIST OF TABLES

Table 1.1: DEFINITIONS **7**

Table 1.2: LIST OF DILATED CARDIOMYOPATHY GENES **11**

Table 1.3: GENETIC LOCI ASSOCIATED WITH LV STRUCTURE **15**

Table 2.1: ECHOCARDIOGRAPHIC BASELINE OF TRANSGENIC MICE **22**

LIST OF FIGURES

Figure 1.1: FIGURE OF THE HEART **3**

Figure 1.2: STEPS OF THE CARDIAC CYCLE **5**

Figure 1.3: VENTRICULAR SEGMENTATION **9**

Figure 1.4: GWAS **13**

Figure 1.5: ASSOCIATION OF MINOR ALLELE WITH MTSS1 EXPRESSION **16**

Figure 1.6: VALIDATION OF MTSS1 LOCUS **17**

Figure 1.7: ASSOCIATION OF MINOR ALLELE WITH CARDIAC TRAITS **18**

Figure 2.1: MICE ANALYZED FOR M-MODE ECHOCARDIOGRAPHY **23**

Figure 2.2: MICE ANALYZED FOR 2D ECHOCARDIOGRAPHY **24**

Figure 2.3: MICE ANALYZED FOR RNA-SEQ **25**

Figure 2.4: TNNT2 R173W iPSC-CARDIOMTOCYTE IMPAIRMENT **28**

Figure 2.5: MTSS1 KNOCKOUT IN iPSC LINES **29**

Figure 2.6: TPM1 CORRECTION IN iPSCs **30**

Figure 2.7: iPSC CARDIOMYOCYTE DIFFERENTIATION PROTOCOL **31**

Figure 3.1: COMBINED SEX DATASET **33**

Figure 3.2: LV STRAIN IN COMBINED SEX DATASET **34**

Figure 3.3: MALE DATASET **36**

Figure 3.4: LV STRAIN IN MALE DATASET **37**

Figure 3.5: FEMALE DATASET **39**

Figure 3.6: LV STRAIN IN FEMALE DATASET **40**

Figure 4.1: M-MODE ECHOCARDIOGRAPHY **42**

Figure 4.2: 2D ECHOCARDIOGRAPHY **48**

Figure 4.3: GENE EXPRESSION QUANTITATION VIA RNA-SEQ **52**

Figure 4.4: GENE EXPRESSION QUANTITATION VIA RNA-SEQ (MALE) **53**

Figure 4.5: GENE EXPRESSION QUANTITATION VIA RNA-SEQ (FEMALE) **54**

Figure 4.6: IMMUNOHISTOCHEMISTRY FOR 3X FLAG MTSS1 EMBRYOS **56**

Figure 4.7: TPM1 EXPRESSION IN TRANSGENIC MICE **57**

Figure 5.1: BEATING RESPONSE RATIO FOR TNNT2 R173W iPSC-CARDIOMYOCYTES **59**

Figure 5.2: BEATING RESPONSE RATIO FOR TPM1 D230N iPSC-CARDIOMYOCYTES **61**

CHAPTER 1: INTRODUCTION

Heart Failure

In 2021, the Heart Failure Society of America, the Heart Failure Association of the European Society of Cardiology, and the Japanese Heart Failure Society formed a committee to develop a consensus definition of heart failure.[1] Traditionally, heart failure was defined around the pathological reduction of cardiac output to levels incapable of sustaining an individual's metabolic requirements.[2] However, such definitions invariably excluded patients who physicians would otherwise agree suffered from heart failure—for example, patients with elevated natriuretic peptide levels or advanced cardiac remodeling. What many definitions agree on is that heart failure is a clinical syndrome; it encompasses an entire constellation of symptoms and signs lumped under the same terminology. Some of these symptoms include the aforementioned increased intracardiac pressure and reduced cardiac output. Others include "dyspnea, fluid retention/edema, fatigue, activity intolerance, and exercise limitation", all alongside some form of heart disease.[1] The committee agreed that existing definitions of heart failure included three separate elements: structural cardiac disease, common heart failure symptoms, and common heart failure signs.

While heart failure is difficult to define with specificity, heart failure's consequences are not. In the United States alone, heart failure was thought to affect over 6 million people in 2020.[3] Globally, around 64 million people were thought to suffer from heart failure in 2017.[4] Heart failure has a 50% median five-year mortality rate and is responsible for over one-third of deaths from cardiovascular causes nationally.[3] Heart failure's prevalence per thousand person-years in African-Americans, Hispanics,

Caucasians, and Asians is 4.6, 3.5, 2.4, and 1.0 respectively.[2] Both the prevalence and cost of heart disease are projected to rise over time; in 2012, the American Heart Association estimated that over 8 million Americans will have heart failure by 2030, with direct medical costs increasing from $21 billion to $53 billion over the same time frame.[5] As a result, both basic and translational research into underlying etiologies leading to heart failure could have clear clinical impact on cardiovascular mortality.

The Heart

The heart is a hollow muscular organ that is responsible for powering circulation of blood throughout an organism's body through rhythmic contraction and dilation **(Figure 1.1)**. In humans (and many other vertebrates), the heart consists of four chambers: two upper chambers—the atria—and two lower chambers—the ventricles. The pulmonary veins connect the left atria to the lungs; the superior and inferior vena cava connect the organs to the right atria; the aorta connects the other organs from the left ventricle, and the pulmonary artery leads to the lungs from the right ventricle. The left ventricle and left atria are separated by the mitral valve, while the right ventricle and right atria are separated by the tricuspid valve. Likewise, the aortic valve controls blood flow from the left ventricle to the aorta, and the pulmonary valve fulfills a similar function between the right ventricle and pulmonary artery. Over the course of one cardiac cycle, deoxygenated blood from the body flows into the vena cavae and through the right atrium and right ventricle, and then is sent to the lungs for oxygenation via the pulmonary artery; freshly oxygenated blood from the lungs flows from the pulmonary veins into the left atrium, then the left ventricle, and out the aorta. As broken into discrete steps **(Figure 1.2)**:[6]

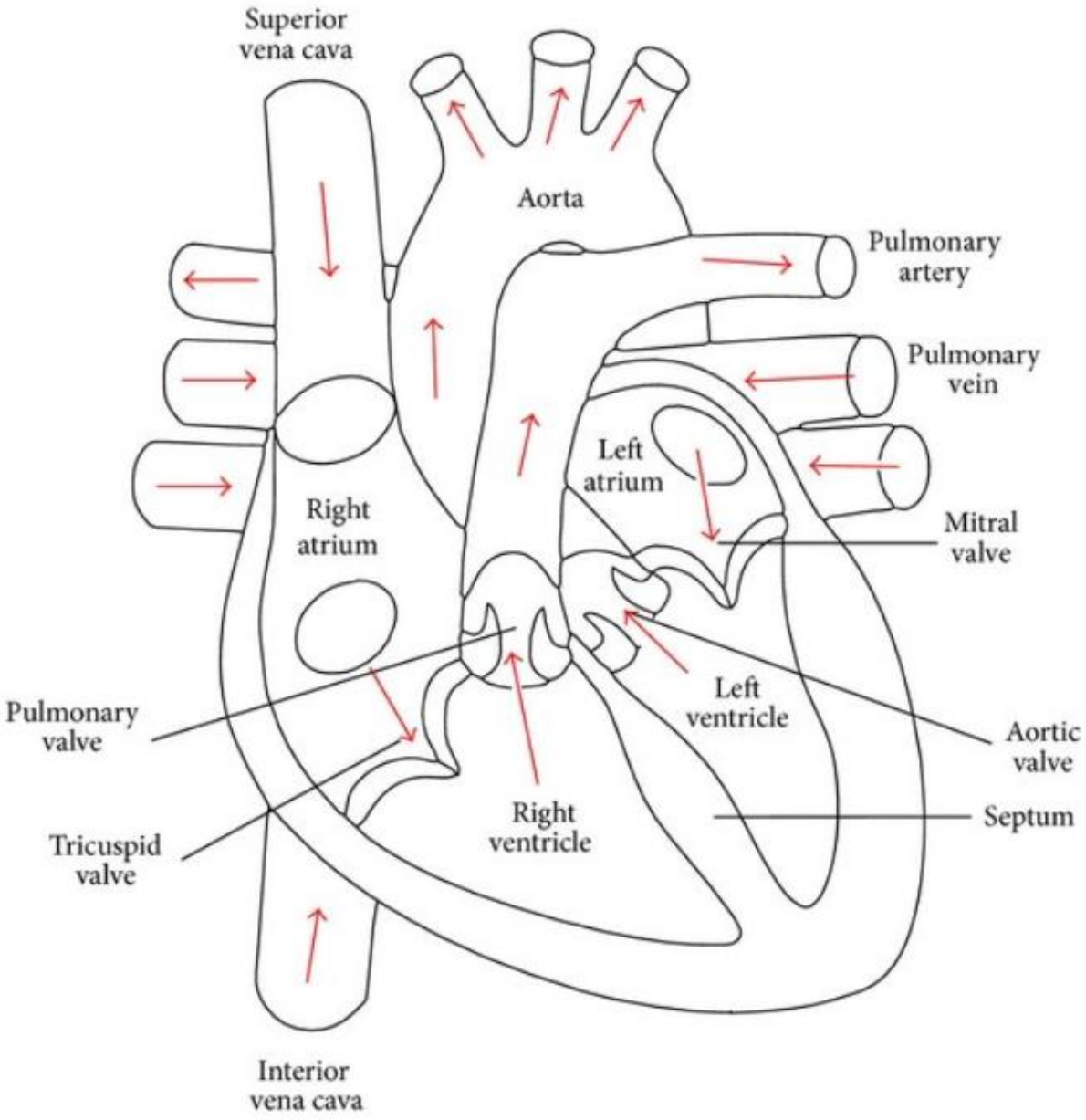

(Figure 1.1) A figure of the heart (transverse section). The arrows denote the directionality of blood flow. Figure adapted from (Sahu et al., 2015).

1: Isovolumetric Relaxation: at the start of the cycle, the aortic valve, pulmonary valve, mitral valve, and tricuspid valve are closed. This allows the ventricular volume to remain constant while cardiac pressure drops to meet atrial pressure, thereby opening the mitral and tricuspid valves.

2: Ventricular Passive Filling: The opening of the mitral and tricuspid valves allows blood from the atria to flow into the right and left ventricles.

3: Atrial Contraction: As ventricular filling slows down, the atria actively contract and increase both volume and pressure in the ventricles. The mitral and tricuspid valves close at the end of this phase. **End Diastolic Volume (EDV)** refers to the total volume of blood in a given ventricle by the end of atrial contraction.

4: Isovolumetric Contraction: With the mitral/tricuspid/aortic/pulmonary valves closed, the heart begins to contract until ventricular pressure reaches that of the pulmonary artery and aorta. This causes the opening of the aortic valve and pulmonary valve.

5: Ventricular Ejection: The ventricles contract and reduce their volume, expelling blood into the pulmonary artery and aorta. The atria relax and increase in volume, thereby collecting blood from the vena cava and pulmonary veins. The final volume of any given ventricle at the end of this phase is known as the **End Systolic Volume (ESV)**. At the very end of this phase, the aortic and pulmonary valve close, thereby setting the conditions for step (1).

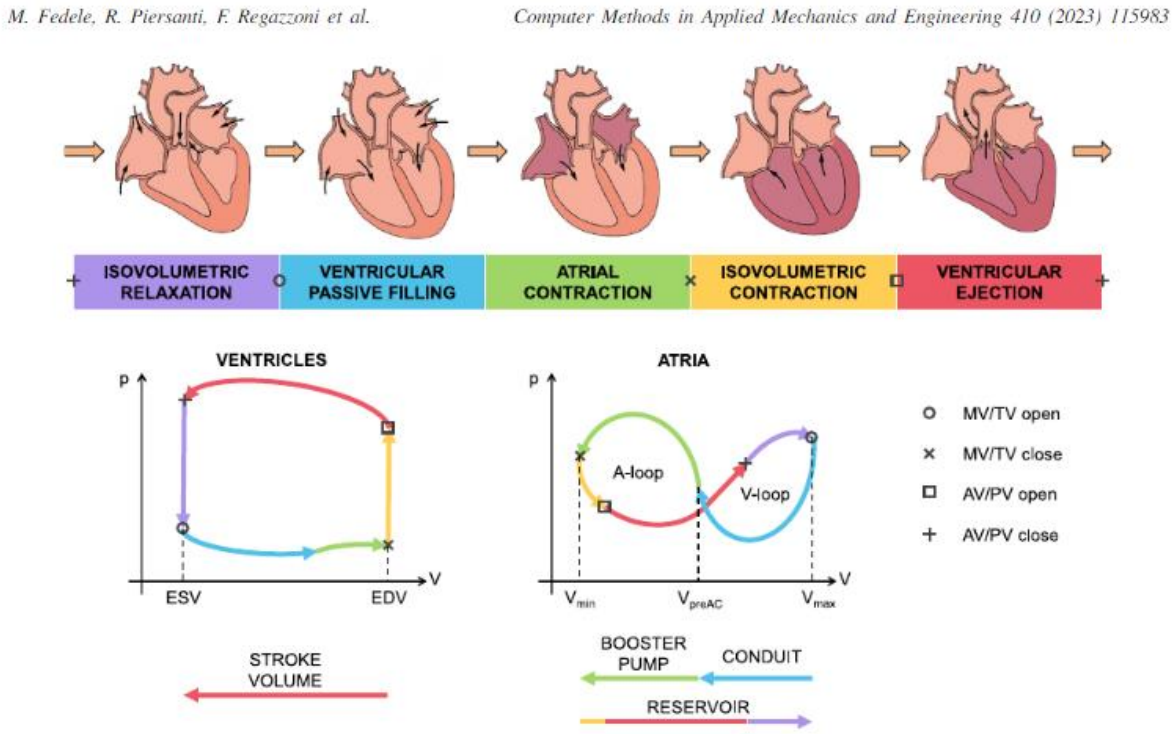

Fig. 2. The five phases of the cardiac cycle: on the top, a sketch of the direction of the blood flow, the status of the valves and the contraction of the chambers (darker color) during the different phases (pictures elaborated from https://commons.wikimedia.org/w/index.php?curid=30148227); on the bottom, schematic ventricular and atrial pressure–volume loops with the opening and closing of the valves and colored with the five phases.

(Figure 1.2): The steps of the cardiac cycle. Figure adapted from (Regazzoni et al., 2023).

In humans, the cardiac cycle repeats roughly 60-100 times per minute under resting conditions; for smaller mammals such as mice, the number may be closer to 500-700.[7,8] The regular and consistent operation of the cardiac cycle must occur at levels capable of sustaining healthy metabolic activity. As a result, defining and quantifying cardiac cycle dynamics and physiology is of utmost importance to the medical community. A list is provided below **(Table 1.1)**, but two require additional detail.

Stroke Volume (SV) is the volume of blood displaced by a ventricle in a single cardiac cycle. While stroke volume typically refers to the left ventricle (and will exclusively refer to the left ventricle in this thesis), right ventricular stroke volume is also a possible measurement.[9,10] Stroke volume is a derived statistic: it

is found by subtracting ventricular volume at its maximum (End Diastolic Volume) from ventricular volume at its minimum (End Systolic Volume).

$$SV = EDV - ESV$$

Ejection Fraction (EF)—specifically, left ventricular ejection fraction—is an important and common indicator of cardiac strength.[11,12] Ejection fraction measures the fraction of blood expelled from the heart in a single cardiac cycle. Much like stroke volume, ejection fraction is also a derived statistic: it is calculated by dividing stroke volume by end diastolic volume, then multiplying the resulting fraction by 100%.[13] Heart failure is often categorized by ejection fraction; while reduction of ejection fraction is a common finding in patients with heart failure (Heart Failure with reduced Ejection Fraction: HFrEF), heart failure can still occur with no change in ejection fraction (Heart Failure with preserved Ejection Fraction: HFpEF).[14,15]

$$EF = (SV / EDV) * 100$$

Name	Calculation	Summary
Body Weight (BW) or Body Mass (BM)		Weight of subject
Cardiac Output (CO)	SV * HR	Total volume of blood pumped per unit time
Ejection Fraction (EF)	(SV / EDV) * 100	Fraction of blood expelled during one cardiac cycle
End Diastolic/Systolic Volume (EDV/ESV)		Volume of blood in ventricle at end of diastole/systole
End Diastolic/Systolic Dimension		Diameter of ventricle at diastole/systole
Left Ventricular Internal Dimension (LVID(s,d))		The diameter of the left ventricle (at a given stage of the cardiac cycle)
Heart Rate (HR)		Number of heart beats per unit time
Fractional Shortening (FS)	(LVID(d) - LVID(s) / LVID(d)) * 100	Percent reduction of ventricle dimension between systole and diastole
Stroke Volume (SV)	EDV-ESV	Volume of blood expelled from heart between diastole and systole

(Table 1.1) A list of definitions used for quantifying cardiac function.

Given the importance of the left ventricle for cardiac function, other quantitative measures have been adopted that assess left ventricular performance. One such measure is myocardial strain: the change in myocardial fiber length over the cardiac cycle.[16] During the cardiac cycle, the left ventricle shortens longitudinally and circumferentially but thickens radially. As a result, left ventricular myocardial strain

can be observed across all three modes of deformation. As heart muscle is not compressible, **left ventricular circumferential strain** (Ecc) practically measures myocardial diameter changes due to wall thickening. This measurement is defined by the change in length of the myocardium along the circumferential axis of the left ventricle; as the myocardium typically shortens in systole, this value is normally negative.[17,18] Unlike the prior measurements, left ventricular circumferential strain can be both measured globally and regionally; by convention, 17 individual elements of the left ventricle across the basal, mid, and apical left ventricle can be measured for circumferential strain **(Figure 1.3).**

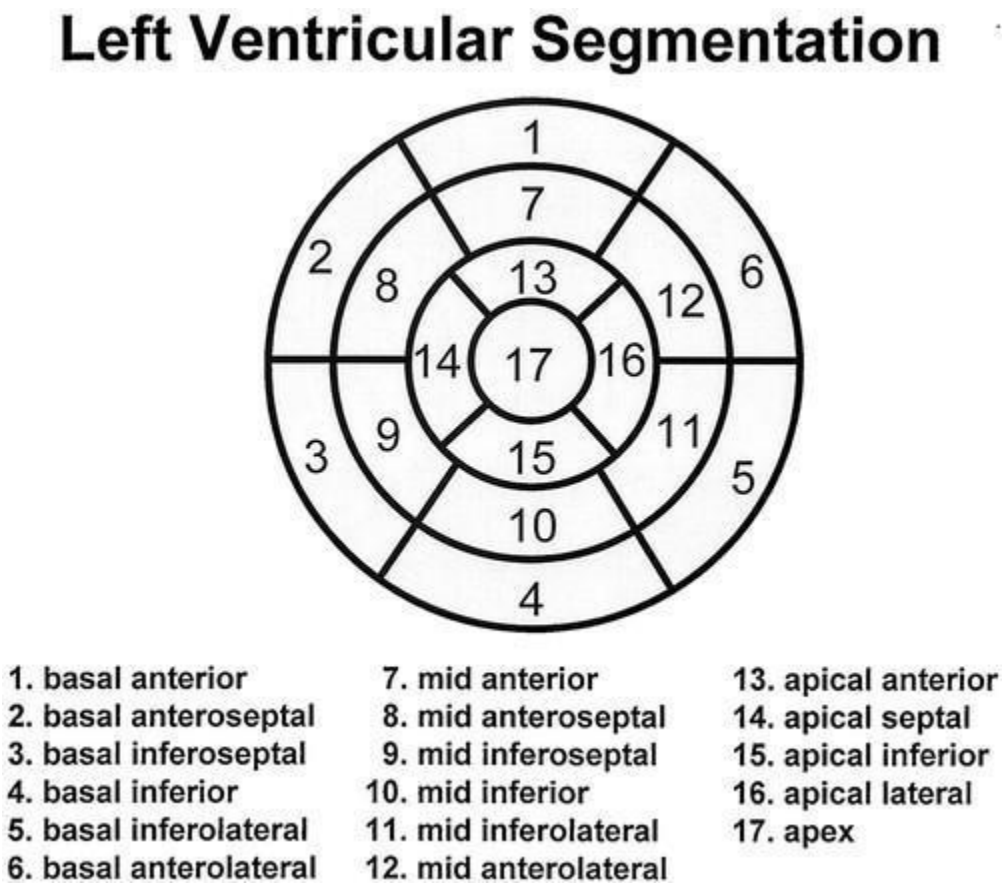

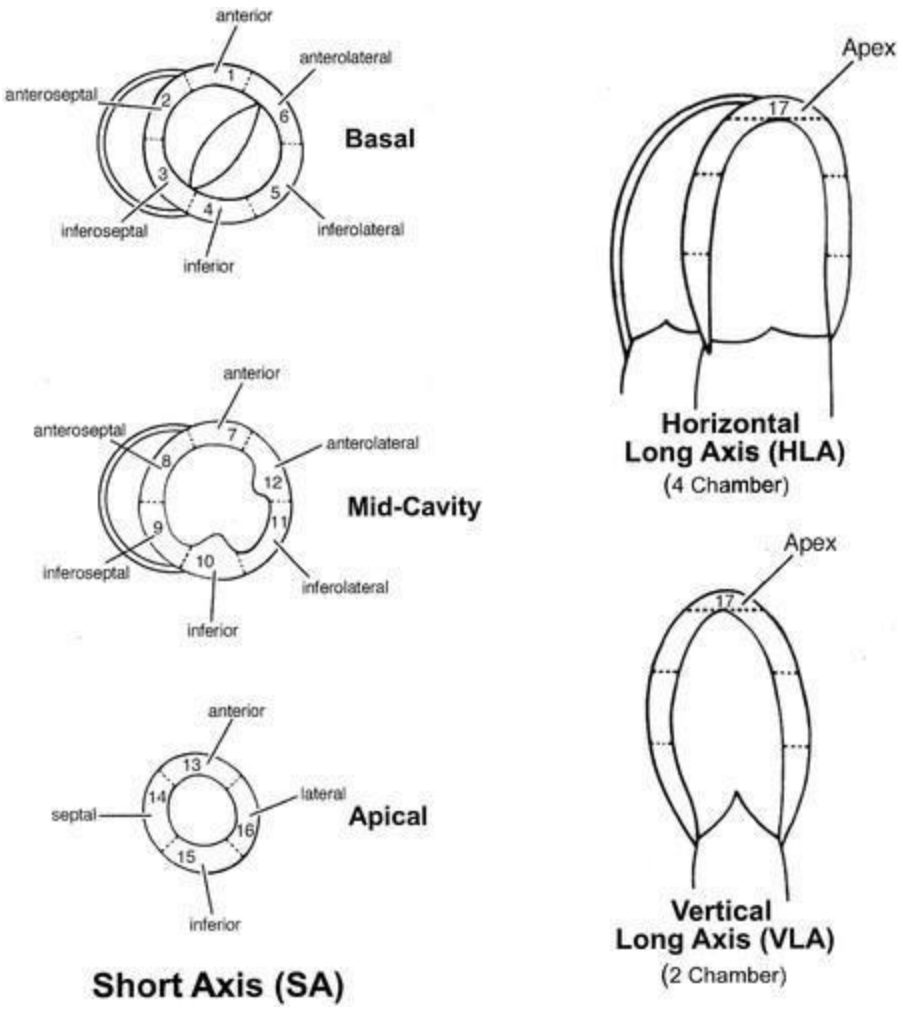

(Figure 1.3) Ventricular segmentation mapping for the left ventricle. The top panel shows the standard American Heart Association polar mapping schematic for segments. Adapted from (Verani et al., 2002).

Dilated Cardiomyopathy

Dilated cardiomyopathy (DCM) is one of the most common causes of heart failure on the planet; its estimated global prevalence in the general population is between 1:250 to 1:2500, and its annual mortality rate is 10,000 people in the United States alone.[19] DCM is characterized by progressive remodeling and enlargement of the left ventricle leading to a reduction in left ventricular ejection

fraction.[20] The majority of DCM cases present in patients between the ages of 20 to 60; DCM is more common in men than women.[21] Signs of DCM can include fatigue, chest pain, palpitations, or shortness of breath.[22] However, the progression of DCM is often asymptomatic—its first manifestation in patients is usually advanced heart failure.[23] While DCM's 5-year survival rate can be as low as 50%, therapeutic intervention can slow disease progression or even trigger reverse remodeling of the left ventricle.[19,23,24]

DCM can be caused by environmental factors such as alcohol abuse or adenovirus infection.[22] However, it is estimated that between 30-40 percent of DCM cases are genetic in nature.[25] Most of these mutations appear to be heritable as autosomal dominant traits. Furthermore, most heritable dilated cardiomyopathies appear to be caused by mutations in genes encoding cytoskeletal, nuclear envelope, or cardiomyocytic sarcomere proteins.[19] A list of the most frequently implicated genes in DCM can be found in **Table 1.2**. However, the search for genes linked to DCM has not been exhaustive and remains ongoing.

Gene	Protein	Estimated prevalence in DCM (%)	Age of onset of DCM (years)	Notes
TTN	Titin	12–25%	DCM: Usually 40–59	- Usually, isolated DCM - More common in women than in men; variable prognosis but family clustering
LMNA	Lamin A/C Nuclear membrane	5–10% (up to 30 if conduction disease also present)	30–49 and penetrance is almost complete at the age of 70; conduction disease usually prominent	- Subset of Emery–Dreifuss muscular dystrophy - Phenotypic expression is characterized by a relatively high incidence of sudden cardiac death or major ventricular arrhythmias, even before the development of systolic left ventricular dysfunction - Class IIa for ICD implantation: NSVT during monitoring, EF <45% at first evaluation, male and non-missense mutations[96][97]
MYH7	β-Myosin heavy chain Sarcomere	4–10%	Variable: adolescence to 49	- Primarily HCM; also, LVNC and RCM - Prognosis variable depending on site of genetic variant; homogeneity within families
MYH6	α-Myosin heavy chain Sarcomere	4%	Variable: adolescence to 49	- Primarily HCM - Prognosis variable depending on site of genetic variant; homogeneity within families
MYPN	Myopalladin Sarcomere, Z-disc	3–4%	Variable: adolescence to 59	- Usually, isolated DCM - Variable presentation with some early deaths due to heart failure
DSP	Desmoplakin Desmosome	3–4%	Variable: mostly 40–49	- ARVC - Identified in multiple patients with advanced DCM although natural history uncertain; arrhythmic burden seems to be much lower than in ARVC
RBM20	RNA-binding protein 20 Spliceosome	1–5%	Adolescence to 50; can present with SCD or advanced heart failure	- Usually, isolated DCM - Rapid progression: SCD and end-stage heart failure are common, with a high incidence of ventricular arrhythmias - Severe disease expression in male patients[98]
TNNT2	Cardiac muscle troponin T Sarcomere	2–3%	Variable: adolescence to 49	- HCM, LVNC, and RCM - Prognosis variable depending on site of genetic variant; homogeneity within families
SCN5A	*SCN5A* (sodium channel protein type 5, α subunit) Ion channel	2–3%	Adolescence	- Brugada syndrome and LQTS - Early onset, commonly with atrial fibrillation; not associated with risk of ventricular arrhythmias
TPM1	α-Tropomyosin Sarcomere	0.5–1.0%	Variable: adolescence to 49	- Other cardiomyopathy: HCM, LVNC, and RCM - Prognosis variable depending on site of genetic variant; homogeneity within families

ARVC = arrhythmogenic right ventricular cardiomyopathy; DCM = dilated cardiomyopathy; EF = ejection fraction; HCM = hypertrophic cardiomyopathy; ICD = implantable cardioverter defibrillator; LQTS = long QT syndrome; LVNC = left ventricular noncompaction; NSVT = nonsustained ventricular tachycardia; RCM = restrictive cardiomyopathy; SCD = sudden cardiac death.

(Table 1.2) A partial list of genes associated with dilated cardiomyopathy. Adapted from (Kim et al., 2021).

Genome-Wide Association Studies

Genome-wide association studies (GWASs) are a research approach designed to identify points of common variation in DNA associated with a trait in question.[26] These studies involve collecting and analyzing genetic data from large populations; some studies involve sequencing reads from well over a

million people.[27] GWASs have become increasingly influential in the search for genetic markers of disease; as of 2021, over 5,700 GWASs have been conducted for over 3,300 traits.[27] These studies have been used to identify genetic loci associated with diseases ranging from obesity to autoimmunity.[28,29]

Although the structure of any given GWAS can vary, the basic framework remains consistent. First, an appropriately sized population needs to be identified for the experiment in question **(Figure 1.4, A)**. This population can either be gathered directly or identified in a previously established biobank. Depending on the nature of the study, this population may be screened for ethnicity, sex, education, and other variables that differentiate them from the general public at large.[27] This population must then be genotyped **(Figure 1.4, B)**. Genotyping can vary from whole genome sequencing to exome sequencing to microarrays that focus principally on common genetic variants, such as single nucleotide polymorphisms; while whole genome sequencing is more thorough, it is also more expensive per person. Like population identification, genotyping data may also be collected from a biobank. Data collected from genotyping must then be processed for further analysis **(Figure 1.4, C and D)**. This can include anonymization, ancestry/relatedness adjustment, rare variant removal, and phenotypic matching with genotyped data.

After these steps, the data can finally be tested for genetic associations **(Figure 1.4, E)**. In this step, each individual genetic variant is tested for association with the experimental phenotype. For binary traits, this is typically done via logistic regression models that compare allele frequencies between cases and controls. For continuous traits, the model is typically linear in nature. Given the multiple testing burden in a genome-wide study, GWASs typically use $P < 5 \times 10^{-8}$ as the testing threshold for statistical significance in studies of common genetic variants; should more data be required to have sufficient

power to achieve statistical significance, additional biobanks or other sources of data can be added to the study **(Figure 1.4, F)**. Replication of results via an untested dataset can also enhance validity of a study before further analysis is conducted **(Figure 1.4, G and H)**.

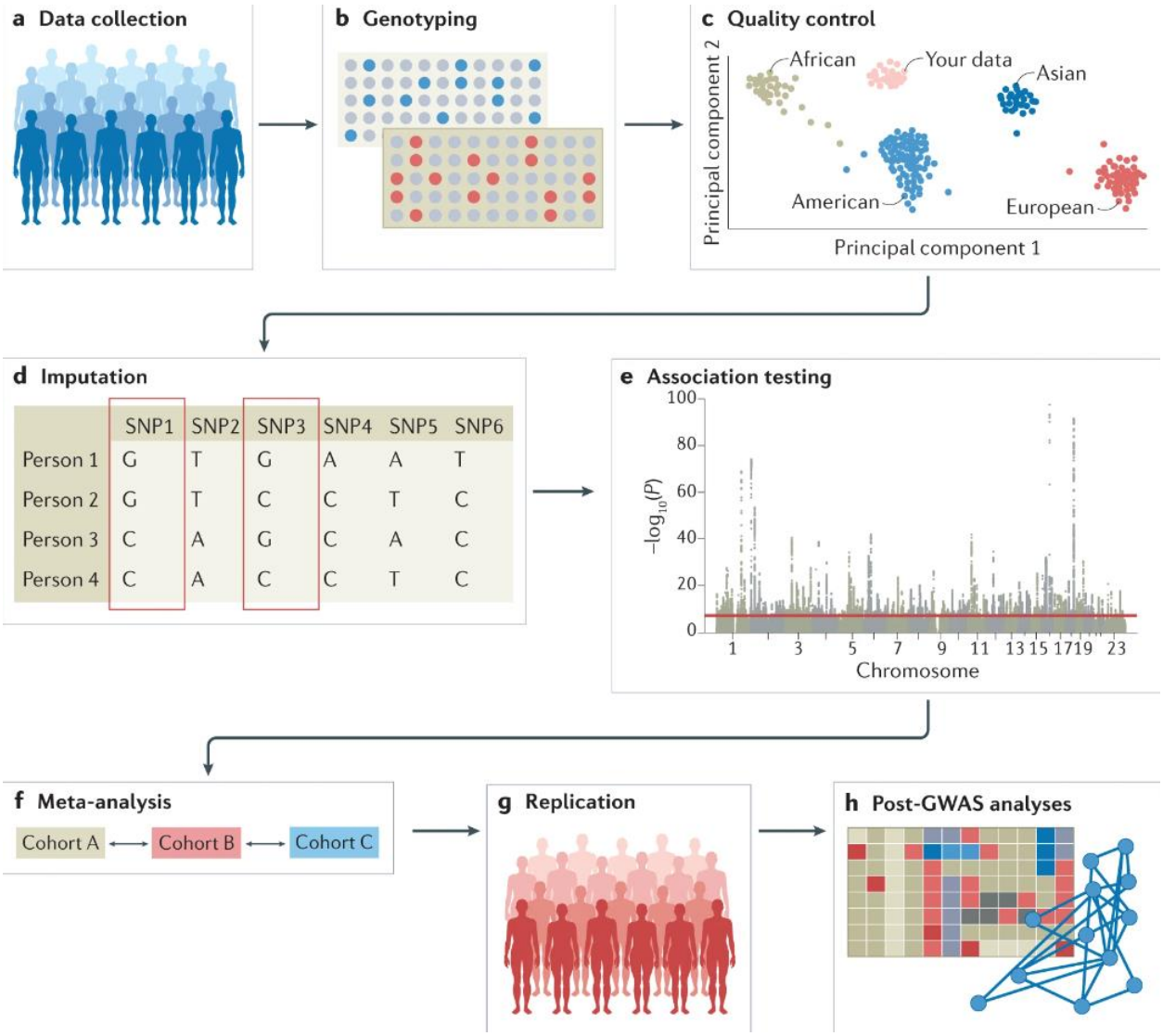

(Figure 1.4) An overview of steps for conducting GWAS. Adapted from (Uffelmann et al., 2021).

Ideally, at the end of this process, a list of genetic variants, their locations in the genome, and their associations with the tested phenotype will be generated. However, this information is not ordinarily enough to prove that any given variant has a causal effect on the phenotype. Linkage disequilibrium—the degree to which one variant is inherited alongside another—may cause noncausal variants to appear highly associated with a phenotype as long as they are disproportionately inherited alongside a causal variant.[30,31] One popular method of correcting for this problem is co-localization; through the combination of a separate expressive quantitative loci (eQTL) study that identifies loci associated with RNA expression in a tissue of relevance with GWAS, it is possible to prioritize variants that affect regulation of relevant genes and also associate with related traits.[27,32]

Multiple studies have used GWASs to identify genetic variants associated with cardiac structural traits that precede heart failure. In 2017, a GWAS meta-analysis using 46,533 subjects from 30 different studies found ten single-nucleotide polymorphisms associated with systolic or diastolic function traits.[33] The genes near these polymorphisms included *MTSS1*, *ATXN2*, *KCNRG*, *CACNA1C*, *PALMD*, *TMEM16A*, *FGGY*, *GOSR2*, *CFDP1*, and *IQCH* **(Table 1.3)**. A separate 2020 meta-analysis focusing on heritable cardiac disease found *MYOZ1*, *SYNPO2L, BAG3,* and *CDKN1A* as significant loci responsible for heart failure.[34] The most recent study covered in this thesis, an analysis conducted in 2022, found loci associated with *DNAJC18, MTSS1, SQLE, BCKDHA, ABO, ALPK3,* and *PROM1* to be most strongly associated with heart failure.[35] However, mass screening of genetic loci can only go so far; individual loci require experimental validation to prove association with suspected gene regulation.

SNP	Chr	Position	Nearest gene	Distance to nearest gene (kb)	SNP annotation	Effect/non-effect allele	EAF[A]	Discovery *P*	Replication *P*	Combined meta-analysis Effect (SEM)	Combined meta-analysis *P*	Combined meta-analysis Heterogeneity I^2	Combined meta-analysis Heterogeneity *P*
AoD (cm)													
rs806322[B,E]	**13**	**49739445**	***KCNRG***	**246.4**	**Unknown**	**A/G**	**0.61**	**6.70×10^{-15}**	**0.035**	**−0.021 (0.003)**	**2.22×10^{-15}**	**0**	**0.620**
rs6702619[C,D,E,F]	**1**	**99818834**	***PALMD***	**65.4**	**Unknown**	**G/T**	**0.50**	**6.89×10^{-15}**	**3.84×10^{-3}**	**0.021 (0.003)**	**$<1.10 \times 10^{-16}$**	**0**	**0.409**
rs10770612[G]	12	20121906	*PDE3A*	291.6	Unknown	A/G	0.80	3.20×10^{-12}	–	–	–	–	
rs17469907[G]	5	122556319	*CCDC100*	152.1	Unknown	A/G	0.72	1.02×10^{-11}	–	–	–	–	
rs1532292[F,G]	17	2044233	*SMG6*	0	Intron	T/G	0.61	1.29×10^{-11}	–	–	–	–	
rs10878359[G]	12	64690891	*HMGA2*	44.6	Unknown	T/C	0.36	1.62×10^{-11}	–	–	–	–	
rs17696696[H]	**16**	**73950853**	***CFDP1***	**0**	**Intron**	**G/T**	**0.59**	**1.96×10^{-9}**	**0.079**	**−0.016 (0.003)**	**2.68×10^{-10}**	**0**	**0.578**
rs7127129[E,F,H]	**11**	**69705561**	***TMEM16A***	**0**	**Intron**	**G/A**	**0.41**	**2.45×10^{-9}**	**0.303**	**−0.015 (0.003)**	**2.44×10^{-9}**	**0.20**	**0.292**
rs17608766[C,D,E,F,H]	**17**	**42368270**	***GOSR2***	**0**	**Intron**	**C/T**	**0.14**	**4.28×10^{-9}**	**0.020**	**0.0244 (0.0038)**	**2.25×10^{-10}**	**0.66**	**0.032**
rs2649	15	61673646	*USP3*	2.9	Untranslated-3′	T/C	0.13	1.01×10^{-8}	0.535	−0.021 (0.004)	5.37×10^{-8}	0.67	0.029
rs4765663	**12**	**2049021**	***CACNA1C***	**0**	**Intron**	**C/G**	**0.16**	**1.39×10^{-8}**	**0.068**	**−0.020 (0.003)**	**4.00×10^{-9}**	**0**	**0.925**
rs11207426[D]	**1**	**59458507**	***FGGY***	**76.8**	**Unknown**	**A/G**	**0.37**	**2.93×10^{-8}**	**0.021**	**0.017 (0.003)**	**2.76×10^{-9}**	**0**	**0.518**
LVDD (cm)													
rs11153730[G]	6	118774215	*SLC35F1*	28.7	Unknown	T/C	0.51	6.40×10^{-16}	–	–	–	–	
rs12541595	**8**	**125926540**	***MTSS1***	**116.7**	**Unknown**	**T/G**	**0.30**	**3.02×10^{-12}**	**4.03×10^{-3}**	**−0.023 (0.003)**	**1.65×10^{-13}**	**0**	**0.513**
rs10774625[D,H]	**12**	**110394602**	***ATXN2***	**0**	**Intron**	**G/A**	**0.50**	**1.90×10^{-8}**	**0.068**	**0.016 (0.003)**	**1.28×10^{-8}**	**0.67**	**0.011**
LVM (g)													
rs1454157	4	177595792	*SPCS3*	108.4	Unknown	C/T	0.73	4.41×10^{-9}	0.301	1.384 (0.260)	9.68×10^{-8}	0.52	0.066
FS (%)													
rs9470361	6	36731357	*CDKN1A*	23.1	Unknown	A/G	0.25	5.30×10^{-9}	0.523	0.169 (0.036)	2.87×10^{-6}	0.62	0.021

[A]From combined meta-analysis. [B]As a proxy for rs2762049, $R^2 = 1.0$, D′ = 1.0. [C]Locus found in discovery phase but not replicated in the previously published meta-analysis (2). [D]Located within enhancer histone marks in ENCODE (17). [E]Located within DNase-hypersensitive sites in ENCODE (17). [F]Locus colocalizes with DEPICT prioritized gene (Supplemental Table 15). [G]Known locus (2), not taken forward for replication. [H]Significantly associated with transcripts in *cis* (see text for details). Chr, chromosome; EAF, effect allele frequency; LVDD, LV diastolic internal dimension; AoD, diameter of the aortic root; FS, fractional shortening. Boldface indicates novel replicated findings. Effects are β coefficients, which represent the change in echocardiographic measure in the units shown in the subheads (i.e., cm, g, or%) per unit difference in effect allele dose.

(Table 1.3) Genetic loci associated with echocardiographic traits of LV structure and systolic function (P < 5.0E-8). Adapted from (Wild et al., 2017).

MTSS1

As alluded to in the previous section, the lead variant rs12541595 in the Metastasis suppressor-1 (*MTSS1*) locus was previously identified as being associated with left ventricular end diastolic dimension in EchoGen.[33] It was also strongly associated with *MTSS1* expression in left ventricular samples collected from individuals of European descent in the Myocardial Applied Genomics Network (MAGNet) consortium.[36,37] After comparison of the association between rs12541595 and *MTSS1* expression across multiple human tissues in the Genotype-Tissue Expression Project, it was discovered that the rs12541595 minor allele was associated with both reduced left ventricular end diastolic dimension and reduced *MTSS1* expression. Further interrogation of the locus via the MAGNet study revealed that rs12541595 marks a cluster of variants that influence left ventricular *MTSS1* expression **(Figure 1.5)**.[36]

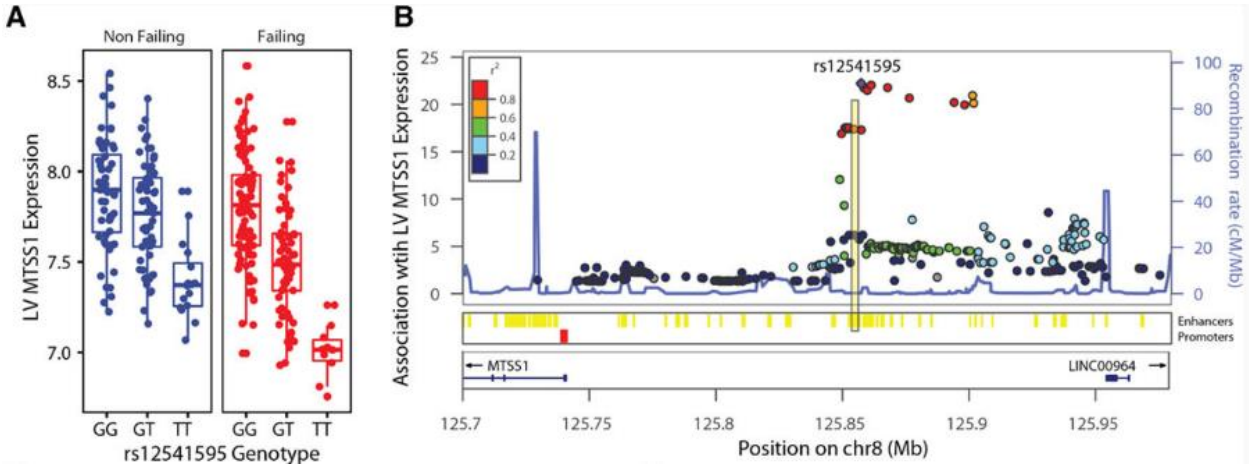

(Figure 1.5) A) association of minor allele (T) with MTSS1 expression in human left ventricle (P = 6E-23). B) cis associations with left ventricular MTSS1 expression. Adapted from (Morley et al., 2019).

Due to these findings, validation of the locus was carried out in animal and cell models. Zebrafish embryos injected with a fluorescent reporter construct containing the 1-kb predicted enhancer region showed high cardiac and myocyte-specific enhancer activity, predominating in the ventricle. Likewise, deletion of the same region in WM266-4 melanoma cells showed reduction of MTSS1 expression **(Figure 1.6)**.

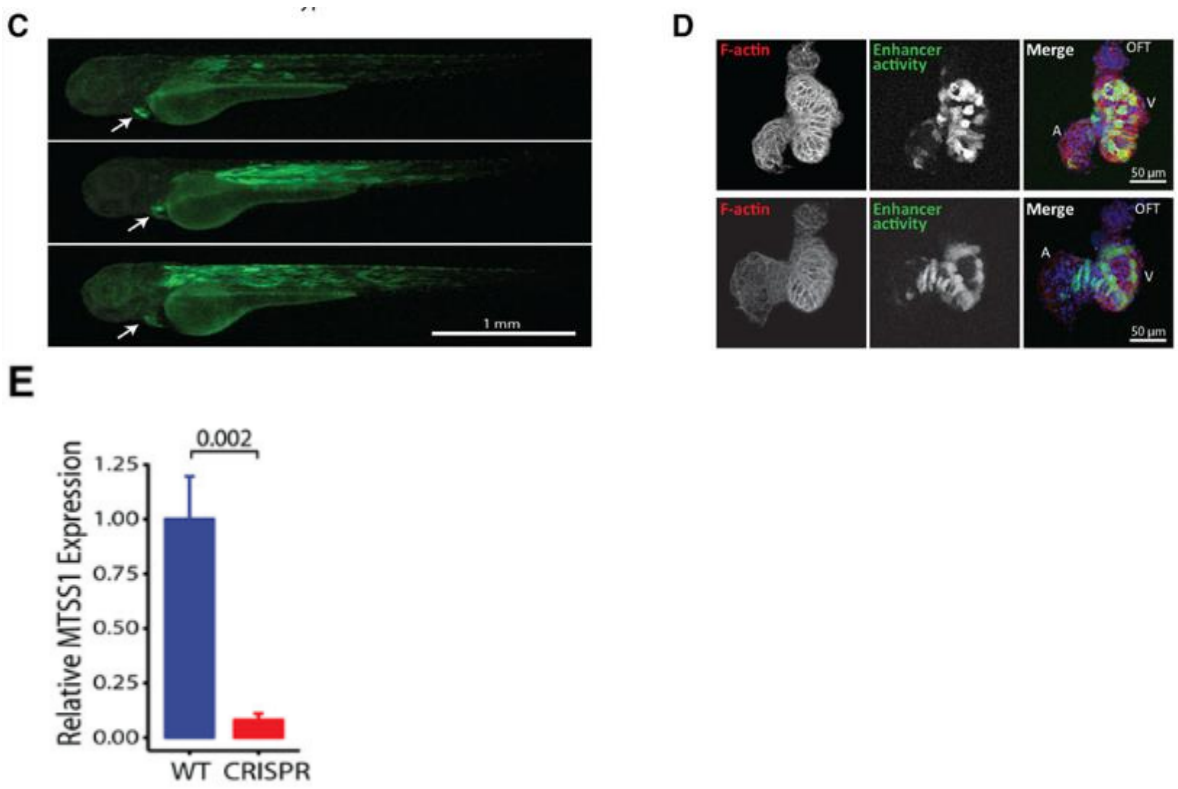

(Figure 1.6) C) Zebrafish embryo containing green fluorescent reporter downstream of enhancer element. D) excised zebrafish heart (ventricle = V, atrium = A, outflow tract = OFT). Nuclei are counterstained blue, sarcomeric actin (F-actin) red. E) CRISPR-Cas9 enhancer deletion in WM266-4 cells. Adapted from (Morley et al., 2019).

The variant rs12541595 was not only linked to cardiac MTSS1 expression and left ventricular dimension; it appeared to be linked to DCM and cardiac health as well. Given a collection of 1540 cases of DCM in patients, an 18% risk reduction per copy of the minor allele was observed ($P = 1 \times 10^{-4}$). The presence of the minor allele was also associated with increased left ventricular fractional shortening ($P = 3 \times 10^{-5}$) and a decrease in left ventricular dimension and mass. A similar trend was detected in a murine model; *Mtss1* knockout mice showed greater fractional shortening and reduced left ventricular dimension than

their wild-type counterparts **(Figure 1.7)**. These results suggested that **cardiac MTSS1 downregulation is cardioprotective**.

H

Disease or Trait	Sample Size	MAF	Beta	OR or HR	P-value
Dilated Cardiomyopathy	5259 (1,540 cases)	0.292	-	0.82	9.95×10^{-5}
All-cause heart failure in the community	20,926 (2,526 cases)	0.302	-	0.96	0.23
LV Mass by EKG voltage					
Leadsum	45772	0.310	-153 mV	-	1.58×10^{-10}
Sokolow	54580	0.308	-28 mV	-	7.97×10^{-7}
Cornell	58424	0.310	-8.8 mV	-	0.014
QRS duration	60025	0.315	-0.092 ms	-	0.14
LV Mass by Echo	27062	0.300	-1.39 g	-	1.16×10^{-5}
LV End-Diastolic Dimension	26950	0.303	-0.026 cm	-	3.02×10^{-12}
LV Wall Thickness	27186	0.301	0.00 cm		0.99
LV Systolic Function by Fractional Shortening	24832	0.301	+ 0.20	-	3.11×10^{-5}
LV Diastolic Function					
E/E'	7463	0.310	+0.0051	-	0.91
E/A	20314	0.318	+0.0061	-	0.04

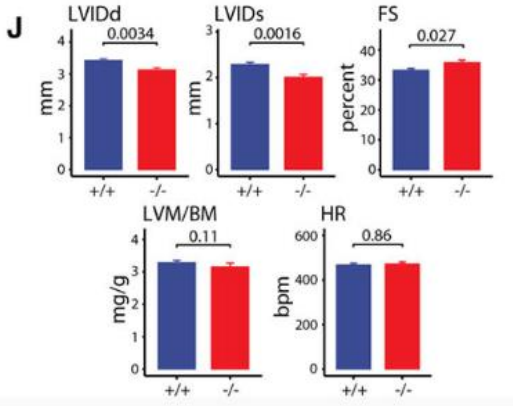

(Figure 1.7) H) Association of minor allele (T) with cardiac traits in sampled human population. J) Echocardiographic measurements of left ventricular traits in *Mtss1*$^{+/+}$ and *Mtss1*$^{-/-}$ mice. LVM = left ventricular mass. Adapted from (Morley et al., 2019).

Unfortunately, the function of MTSS1 in cardiac tissue has remained unclear. MTSS1 was originally known as Missing in Metastasis (MIM); as the name implies, MTSS1 is best known as a tumor suppressor that reduces cell proliferation/invasion in breast, bladder, and kidney cancer cells.[38,39,40] Structurally, MTSS1 appears to be a multifunctional scaffold protein.[41] MTSS1 possesses an I-BAR domain that can bind and deform cellular membranes; it may also interact with actin through a WH2 domain and affect multiple actin cytoskeleton regulatory proteins such as Rac1 GTPase or cortactin.[41] Overexpression of MTSS1 can lead to changes in cell morphology such as filopodia and lamellipodia.[42] MTSS1 appears to act at the interface of the plasma membrane and cytoskeleton, influencing cell morphology and cellular interactions.[41] How, if at all, MTSS1's function protects against heart failure has remained unknown.

Despite demonstration of MTSS1's impact on physiological phenotypes associated with improved left ventricular health, it has remained unclear whether MTSS1 downregulation has a protective effect against genetic DCM *in vivo* or *vitro*. Nor has the mechanism of this effect been studied. In this thesis, I attempted to do both.

CHAPTER 2: METHODS

Bioinformatics

We wanted to test whether cardiac traits associated with *MTSS1* downregulation are consistent across both male and female populations. To do this, we performed a genetic association study between the *MTSS1* lead SNPs and the MRI cardiac traits from the UK Biobank using PLINK2 (version 2.0). 10,895 men (mean ± SD age 55.8 ± 7.5 years) and 11,476 women (54.4 ± 7.2 years) underwent genotyping and cardiac magnetic resonance (CMR) imaging; associations between 82 CMR traits and variants within 100 kb of the *MTSS1* enhancer at chr 8:124845117 were fine-mapped and tested independently using the below additive model.

CMR trait ~ *MTSS1* SNP + sex + weight + height + age + PC1:PC10

PC1 through PC10 were integrated as covariates in order to adjust for genetic backgrounds.

To better understand whether the lead *MTSS1* SNPs regulated gene expression levels, we extracted the expression quantitative trait loci (eQTLs) of the lead *MTSS1* SNPs from the Genotype-Tissue Expression

project (GTEx, v8 release) (https://gtexportal.org/home/).[37] Data were derived from left ventricular samples taken from subjects of European ancestry. The data can be downloaded here:

https://console.cloud.google.com/storage/browser/gtex-resources

To determine whether the above two association studies were colocalized, we performed colocalization analysis using the coloc package (version 5.2.2) (https://cran.r-project.org/web/packages/coloc/index.html). We computed the probability that each CMR trait and the *MTSS1* expression level were associated and shared a single causal SNP using the function coloc.abf(). We focused on the region of 10^5 bases upstream and downstream of the lead SNP rs12541595. We harmonized the GWAS results from human genome version hg19 to human genome version hg38 using MetaXcan (https://github.com/hakyimlab/MetaXcan/wiki/Tutorial:-GTEx-v8-MASH-models-integration-with-a-Coronary-Artery-Disease-GWAS).

After finishing the mixed-sex analysis, we stratified the subjects in UK Biobank by sex and repeated the above analyses. We did not stratify the eQTL data by sex; according to the GTEx expression data, sex does not significantly impact *MTSS1* expression.[43]

Murine Genetic Model

We wanted to test whether MTSS1 downregulation would result in cardioprotective effects in a mouse model of human cardiomyopathy. We already possessed a characterized C57BL/6 global *Mtss1* knockout (KO) mouse, previously generated by the Musunuru lab.[36] However, we required a genetic DCM mouse

model that shared the same genetic background as the *Mtss1* knockout mouse, manifested DCM traits reliably, and had previously been characterized.

We settled on a transgenic DCM mouse model previously created by Dr. Jill Tardiff's laboratory.[44] The Tardiff laboratory had linked the D230N point mutation in alpha tropomyosin (*TPM1*) with severe DCM in two separate human families; to create their genetic model, a *Tpm1* D230N transgene was inserted into mouse embryos of the FVB inbred strain via pronuclear injection. These mice were then backcrossed onto the C57BL/6J inbred strain for over ten generations.

The following primers were used for genotyping of the mice:

- Forward *Mtss1* WT primer: AGCATATCCCCACCCATGTT
- Reverse *Mtss1* WT primer: CCCCGGCATCTTTGTACACT
- Forward *Mtss1* KO primer: AGTCACATCTTGGTGGACGC
- Reverse *Mtss1* KO primer: GGTAGCCCCATGACAGAAGG
- Forward *TPM1* D230N primer: ACCTAGAGGGAAAGTGTCTT
- Reverse *TPM1* D230N primer: AGTTCATCTTCAGTGCCCTT

The resulting C57BL/6J *Tg(Myh6-Tpm1*D230N)*$^{Tg/0}$ mice consistently manifested a progressive DCM phenotype. As quantified by echocardiography, *Tg(Myh6-Tpm1*D230N)*$^{Tg/0}$ mice showed greater left ventricular systolic and diastolic dimensions, end-diastolic volume, and end-systolic volume than their wild-type counterparts by two months of age **(Table 2.1)**. The same transgenic mice also demonstrated lower ejection fraction and fractional shortening.

Summary of Echocardiographic Parameters obtained at 2 and 6 months for mixed gender D230N-Tm hearts. Left ventricular internal diameter in diastole and systole ($LVID_d$ and $LVID_s$ respectively), end diastolic volume (EDV), end systolic volume (ESV), ejection fraction percent (%EF), fractional shortening percent (%FS), cardiac output (CO).

	2 Months		6 Months	
	Non-Tg	D230N-Tm	Non-Tg	D230N-Tm
$LVID_d$(mm)	3.74 ± 0.05	4.03 ± 0.06**	3.84 ± 0.89	4.38 ± 0.08**
$LVID_s$ (mm)	2.28 ± 0.08	2.96 ± 0.16**	2.51 ± 0.11	3.36 ± 0.17**
EDV (µl)	59.73 ± 1.76	71.41 ± 2.55**	64.73 ± 4.37	87.01 ± 3.89**
ESV (µl)	18.02 ± 1.58	34.30 ± 4.60**	23.49 ± 2.95	46.78 ± 6.02*
% EF	69.81 ± 2.41	51.83 ± 6.01**	67.11 ± 3.68	46.78 ± 4.42**
% FS	38.92 ± 1.97	26.51 ± 3.84**	37.03 ± 2.97	23.52 ± 2.57**
CO (ml/min)	15.33 ± 1.66	17.66 ± 3.1	15.52 ± 1.73	15.11 ± 0.97

(Table 2.1) Echocardiographic measurements of transgenic mice. *: P less than or equal to 0.05, **: P less than or equal to 0.01. Adapted from (Lynn et al., 2017)

As we planned on using echocardiography as the primary readout, we obtained the above transgenic mice and crossed them with our *Mtss1* knockout mice for our murine experiments. *Mtss1* knockout mice were genotyped as previously described; the same is true for the transgenic DCM mice.[36,44] All animal experiments described in this thesis were performed according to institutional guidelines and were approved by the University of Pennsylvania Institutional Review Board.

M-mode Echocardiography

Mice from the above-mentioned crosses were subjected to echocardiography at 4.4-5.6 months of age **(Figure 2.1)**. Due to the large number of mice to be analyzed and limitations in equipment and personnel availability, it was not possible to analyze all mice at exactly the same age. Ultrasonographic

examination was performed by the Mouse Cardiovascular Phenotyping Core. Echocardiograms were acquired using a Vevo 2100 Fujifilm VisualSonics Ultrasound System. Mice were anesthetized with an intraperitoneal injection with ketamine, then were taped onto a heated pad after hair removal. Echocardiograms were acquired by a blinded echocardiography technician. M-mode images were recorded, then analyzed using Vevo Lab Software (VisualSonics). The resulting data was graphed via GraphPad Prism. Statistical significance was assessed by Tukey's Post-Hoc test.

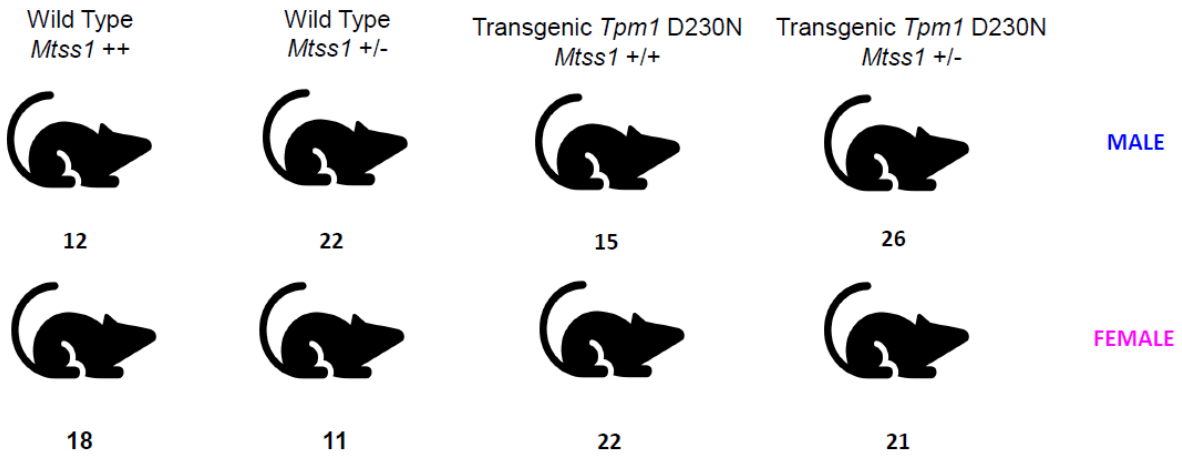

(Figure 2.1) Genotypes and quantities of mice analyzed with M-mode echocardiography.

2D Echocardiography

2D echocardiographic images were captured at the same time as M-mode echocardiography for future analysis. These images were analyzed by the Mouse Cardiovascular Phenotyping Core for additional information. All personnel involved in image analysis were blinded. Some images were lost due to corrupted data before analysis; as a result, the number of mice per group for 2D echocardiography do not match those of M-mode echocardiography **(Figure 2.2)**. The resulting data was graphed via GraphPad Prism. Statistical significance was assessed via Tukey's Post-Hoc test.

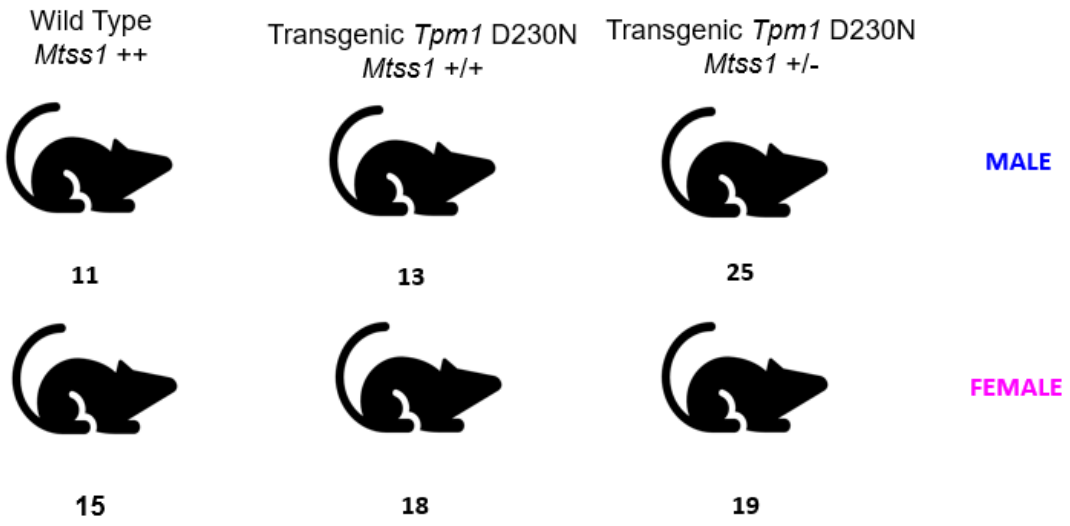

(Figure 2.2) Genotypes and quantities of mice analyzed for 2D echocardiography.

RNAseq

We collected left ventricular tissues from mice sacrificed at around 5 months of age **(Figure 2.3)**. These tissues were flash frozen in liquid nitrogen and were sent to Genewiz for RNA extraction and RNA sequencing (RNAseq). As some samples were swapped during this process, sample verification was conducted via RT-qPCR for *Mtss1* or *Tpm1* count after RNAseq. Paired-ended RNAseq reads were aligned to the mouse reference genome (mm10) using STAR (version 2.7.9a).[8] Fastqc (version 0.11.7) (https://www.bioinformatics.babraham.ac.uk/projects/fastqc/) was used to check the quality of the reads. Picard (https://broadinstitute.github.io/picard/) was then used to mark duplicates, compute RNAseq metrics and estimate library complexity. We then calculated the raw read counts using the Rsubread package (version 2.0.3). Genes where 25% of samples had less than one count per million

were removed from further analysis. We used the voom function from the Limma package (version 3.56.1) to transform/normalize the data, and the toptable function to output the differential analysis result. GraphPad Prism was used to plot the resulting data.

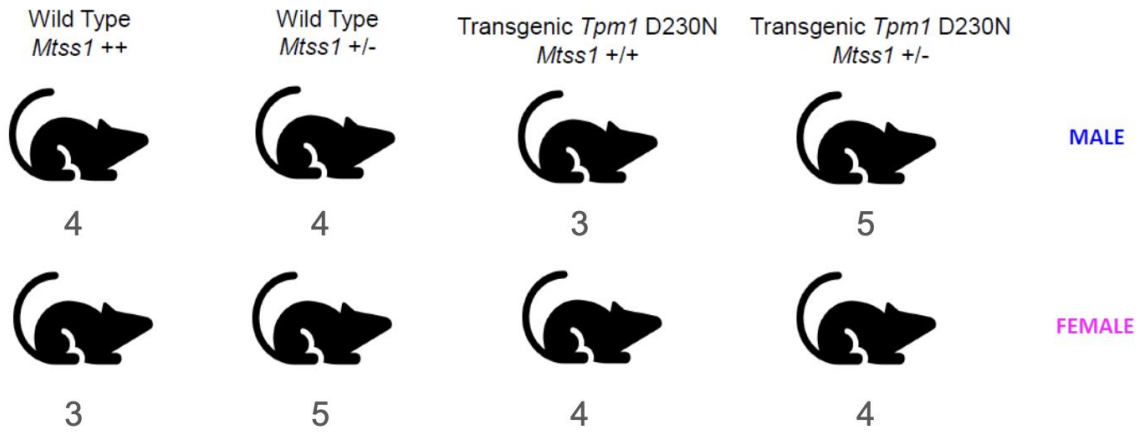

(Figure 2.3) Genotypes and quantities of mice analyzed for RNASeq.

FLAG Immunohistochemistry

In order to assess *Mtss1* localization and expression, we generated a tagged *Mtss1* variant. We decided to add a 3× FLAG tag to either the C-terminus or N-terminus of the sequence encoded by *Mtss1*. *Mtss1* 3× FLAG C-terminus and 3× FLAG N-terminus mice were created by the University of Pennsylvania Transgenic Mouse Core via CRISPR-mediated homology-directed repair in C57BL/6J mouse embryos. Unfortunately, 3× FLAG N-terminus mice demonstrated embryonic lethality and thus were unusable. However, the 3× FLAG C-terminus mice were viable; the below experiment was conducted using this model.

Male mice heterozygous for the 3× FLAG allele were mated with female mice heterozygous for the 3× FLAG allele. Female mice were sacrificed for whole embryo extraction at day E14.5. Embryos were then fixed in 10% paraformaldehyde and sent to the Penn Cardiovascular Institute Histology Core for sagittal sectioning and immunohistochemistry. Visualization and image capture was performed using a Keyence BZ-X800 Microscope with a TRIT-C filter cube.

The following primers were used for genotyping of the mice:

- Forward FLAG N-terminus primer: CGGTTTTCTCTGCACCAAGA
- Reverse FLAG N-terminus primer: GACTCTTTCCTGCAGCCAAG

Reverse Transcriptase Quantitative Polymerase Chain Reaction (RT-qPCR)

Left ventricular tissue was taken from mice at around 5 months of age. This tissue underwent homogenization and RNA extraction via a Qiagen RNEasy Kit. Extracted RNA then underwent reverse transcription with random hexamers and was quantified with TaqMan Gene Expression Assays for murine *Tpm1* (Thermo Fisher Scientific Mm00460614_m1, #4448892) and *Gapdh* (Applied Biosystems #4351309). *Tpm1* expression was normalized against *Gapdh* expression. The resulting data was graphed via GraphPad Prism. Statistical significance was assessed via the Student t-test (wild-type male vs. wild-type female, Tg male vs. Tg female, Tg male vs. wild-type male, Tg female vs. wild-type female).

Human Induced Pluripotent Stem Cell-Derived Cardiomyocyte Genetic Models

While murine models phenocopy the pathogenic effects of DCM reasonably well, mice are biologically distinct from humans. As a result, we wanted to test MTSS1 downregulation in a genetically human *in vitro* system. Much like our *in vivo* experiments, we sought genetic DCM models. For our *in vitro* experiments, we settled on two such models; troponin T (*TNNT2*) R173W human induced pluripotent stem cell (iPSC)-derived cardiomyocytes, and TPM1 D230N iPSC-derived cardiomyocytes.

The *TNNT2* R173W iPSC-cardiomyocyte model had previously been generated and characterized by the Dr. Joseph Wu's laboratory.[45] The *TNNT2* R173W mutation had been discovered in a three-generation family carrying the aforementioned point mutation. iPSCs were generated from patients in this family, then differentiated into iPSC-cardiomyocytes. Relative to familial control iPSC-cardiomyocytes, *TNNT2* R173W iPSC-cardiomyocytes showed impaired response to beta-adrenergic stimulation; they exhibited blunted spontaneous beating rates after isoproterenol addition **(Figure 2.4)**.[45]

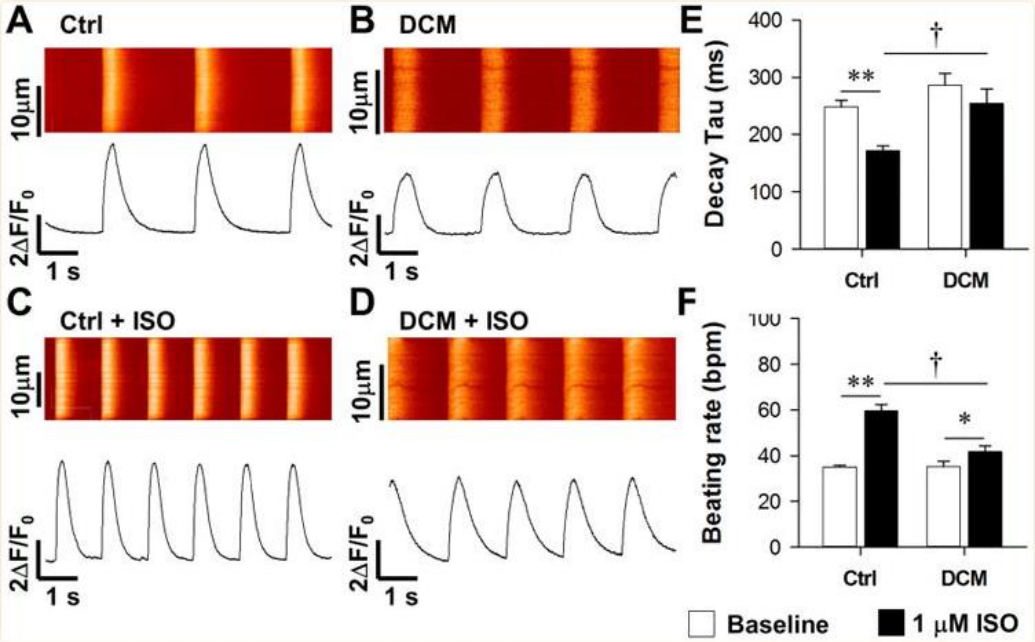

(Figure 2.4) A-B) Representative recording of spontaneous calcium transient of control and TNNT2 R173W iPSC Cardiomyocytes. C-D) As A-B, excepting the addition of 1 uM isoproterenol. E) Decay Tau (ms) before and after isoproterenol addition. F) Beating rate before and after isoproterenol addition. †: $P < 0.05$, **: $P < 0.01$. Adapted from (Wu et al., 2015).

Following the publication of the Wu laboratory's work, the Musunuru laboratory introduced the *TNNT2* R173W mutation into the male-karyotype DiPS 1016 SevA iPSC line via genome editing.[46] For our studies, we used Cas9 with two guide RNAs to knock out *MTSS1* via excision of exon 1 in this iPSC line **(Figure 2.5)**. Editing and selection of *MTSS1* knockout iPSCs was performed according to a previously described protocol.[47] We ultimately used three isogenic iPSC lines: the original wild-type DiPS 1016 SevA iPSC line, the *TNNT2* R173W line, and the *TNNT2* R173W *MTSS1* knockout line.

	CRISPR Guide RNA Sequence
5' Guide RNA	AACCAGCCGCGCGAGCTGGC**TGG**
3' Guide RNA	GCCGAGTTCGATAAAGTTGC**AGG**

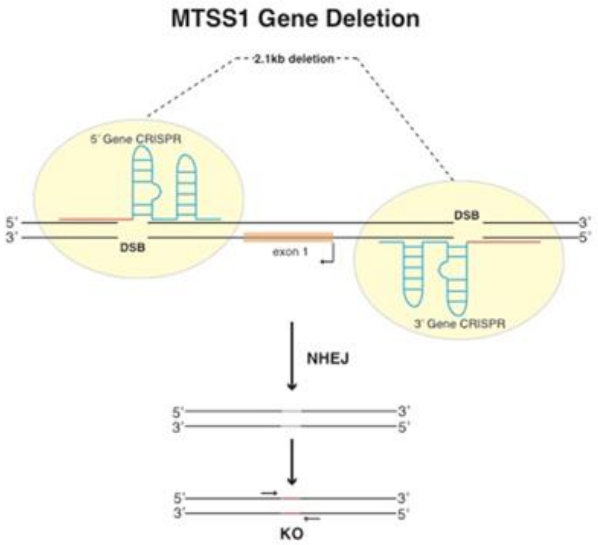

Forward WT primer: AGTCACATCTTGGTGGACGC
Reverse WT primer: AGTCACATCTTGGTGGACGC

Forward KO primer: AGTCACATCTTGGTGGACGC
Reverse KO primer: AGTCACATCTTGGTGGACGC

(Figure 2.5) Schematic of MTSS1 knockout in iPSC lines via Cas9.

In consultation with the Penn Center for Inherited Cardiovascular Disease, we learned that two female DCM patients receiving care at the Center possessed the *TPM1* D230N mutation. Under the Center's IRB-approved protocol, iPSCs were generated from these patients by the Penn Cardiovascular Institute iPSC Core. One of these iPSC lines underwent Cas9-mediated *MTSS1* knockout. The same iPSC line underwent correction of the *TPM1* D230N mutation back to its wild-type analogue via Cas9-mediated

homology directed repair with a DNA template **(Figure 2.6)**. We ultimately used three iPSC lines: the corrected *TPM1* line (wild-type), the original pathogenic *TPM1* D230N line, and the *TPM1* D230N *MTSS1* knockout line.

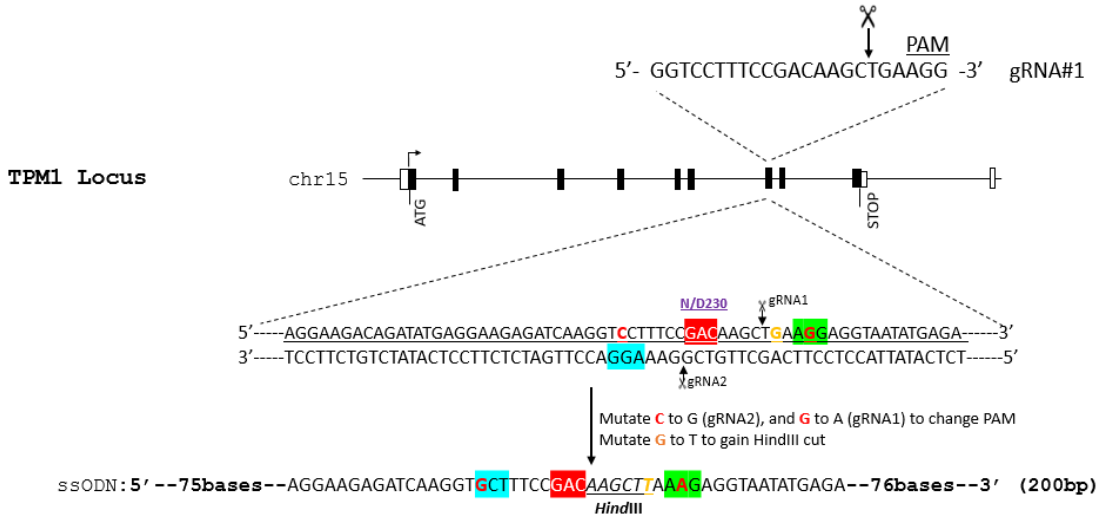

Donor ssODN
5'-
gagtagattgagctgcagcctgacatctggaatgctctttctaattacagtactcgcagaaggaagacagatatgaggaagagatcaaggtGctttccg
ac*aagctT*aaAgaggtaatatgagagttgtggatgaagccaactggattttaaatgagtttgttttcatggaaccggtcagggccttttcattttaaagtt
-3'

aGg -> aAg: Mutation of PAM#1
Cct -> Gct: Mutation of PAM#2
aagctG -> aagctT: Gain of *Hind*III

gRNA#1: 5'-GGTCCTTTCCAACAAGCTGA-3'
gRNA#2: 5'-CCTCCTTCAGCTTGTTGGAA-3'

(Figure 2.6) *TPM1* was corrected back to its non-pathogenic form for use in downstream experiments. First, Cas9 was used to cut DNA directly upstream and downstream of the D230N mutation. Donor single-stranded oligodeoxynucleotides were used to repair the resulting cut, correcting the affected amino acid from N to D. The donor strand also introduced synonymous mutations to both guide RNA protospacer-adjacent motif sites, preventing cuts after correction. A HindIII site was also introduced for ease of screening corrected iPSCs.

Isoproterenol Assay

TNNT2$^{R173W/+}$*MTSS1*$^{+/+}$, *TNNT2*$^{R173W/+}$*MTSS1*$^{-/-}$, and *TNNT2*$^{+/+}$*MTSS1*$^{+/+}$ iPSC lines were differentiated into iPSC-cardiomyocytes per the described protocol **(Figure 2.7)**.[48] Individual cardiomyocytes were then patch-clamped. 1 µM isoproterenol was then added to the patch-clamped cells. The cardiomyocyte spontaneous beating rate was recorded before isoproterenol addition, as well as ten minutes after isoproterenol addition. *TPM1*$^{D230N/+}$*MTSS1*$^{+/+}$, *TPM1*$^{D230N/+}$*MTSS1*$^{-/-}$, and *TPM1*$^{+/+}$*MTSS1*$^{+/+}$ cells were also differentiated and patch-clamped per the same protocol. Data was visualized via GraphPad Prism. Statistical significance was determined using Tukey's Post-Hoc Test.

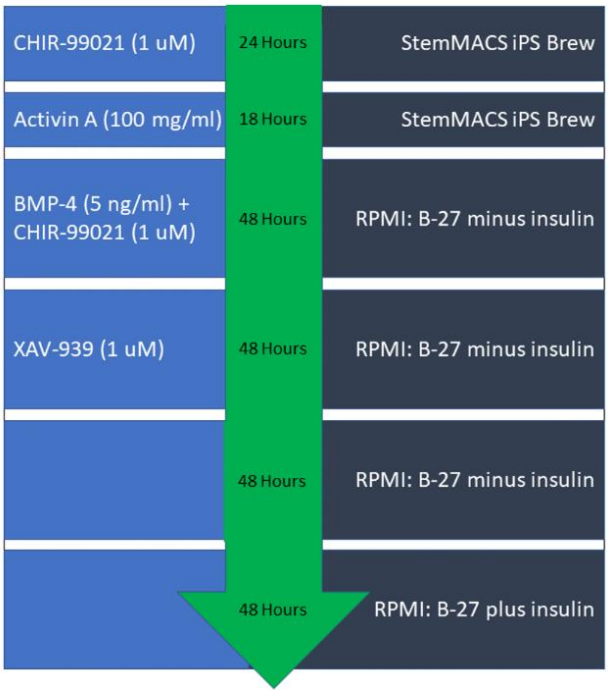

(Figure 2.7) A schematic of the cytokines and media used in the iPSC-cardiomyocyte differentiation protocol.

CHAPTER 3: BIOINFORMATICS

Combined Dataset

For the complete dataset **(Figure 3.1)**, fine-mapped association analysis shows that left ventricular *MTSS1* enhancer variants are associated with cardiac magnetic resonance (CMR) phenotypes such as global left ventricular circumferential strain (Ecc_Global), left ventricular ejection (LVEF), left ventricular end-systolic volume (LVESV), and left ventricular end-diastolic volume (LVEDV). Colocalization analysis between GWAS associations and GTEx human left ventricular *MTSS1* expression reveals strong colocalization between *MTSS1* variants, *MTSS1* expression, and CMR phenotypes. *MTSS1* expression reduction is linked to higher LVEF, lower LVESV, lower LVEDV, and lower global left ventricular circumferential strain (ColocPR: LVEF = 0.994, LVESV = 0.993, LVEDV = 0.764, Ecc_Global = 0.995). Multiple local left ventricular segments concentrated in the apical and mid septal through inferior regions—plus the basal inferior region—also showed strong linkages (ColocPR: Ecc_AHA_14 = 0.993, Ecc_AHA_9 = 0.993, Ecc_AHA_10 = 0.980, Ecc_AHA_7 = 0.960, Ecc_AHA_4 = 0.915, Ecc_AHA_15 = 0.908, Ecc_AHA_8 = 0.865, Ecc_AHA_3 = 0.865) **(Figure 3.2)**.

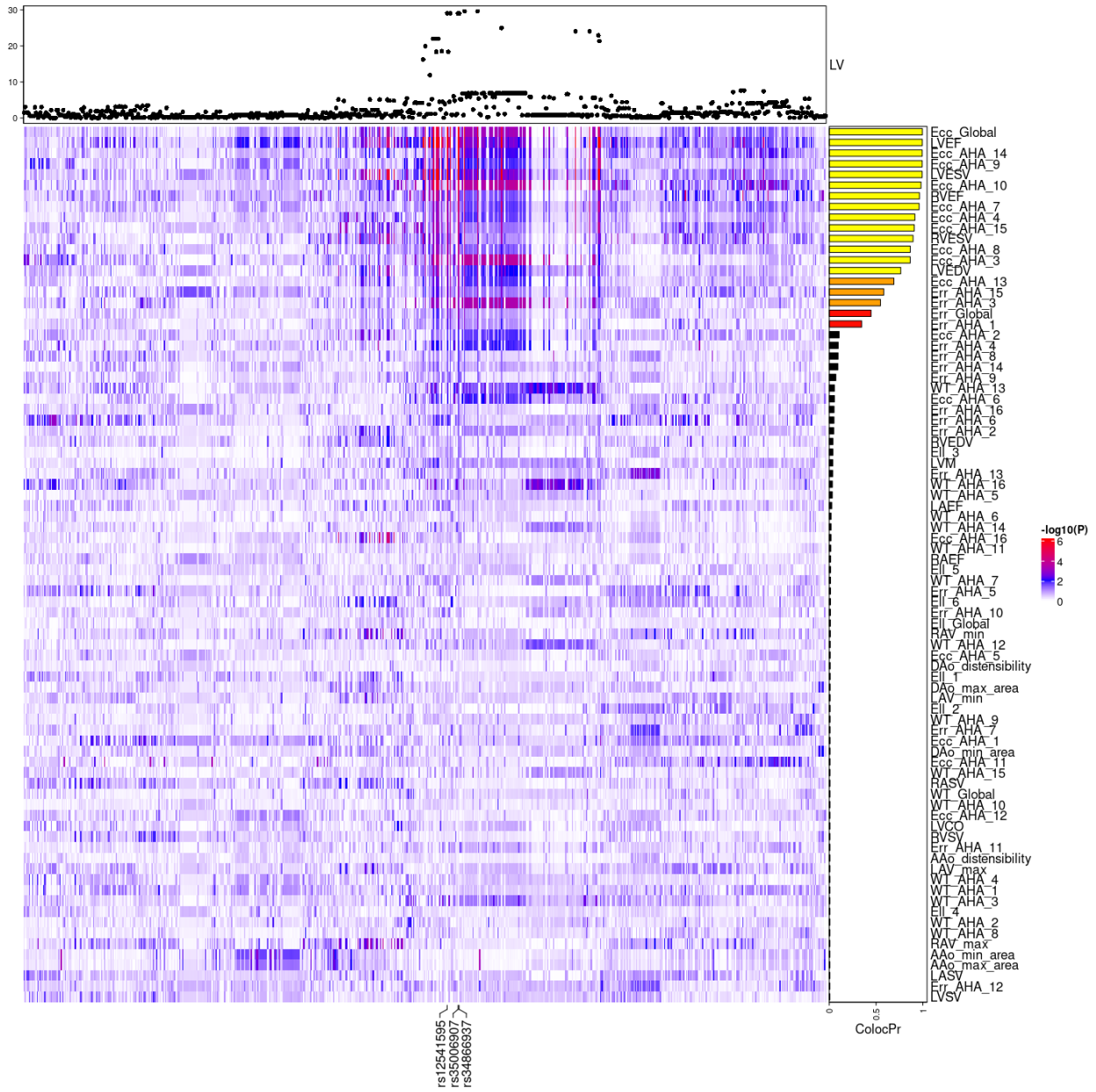

(Figure 3.1) Association of *MTSS1* enhancer variation with CMR traits and colocalization with *MTSS1* expression in GTEx for the combined sex dataset.

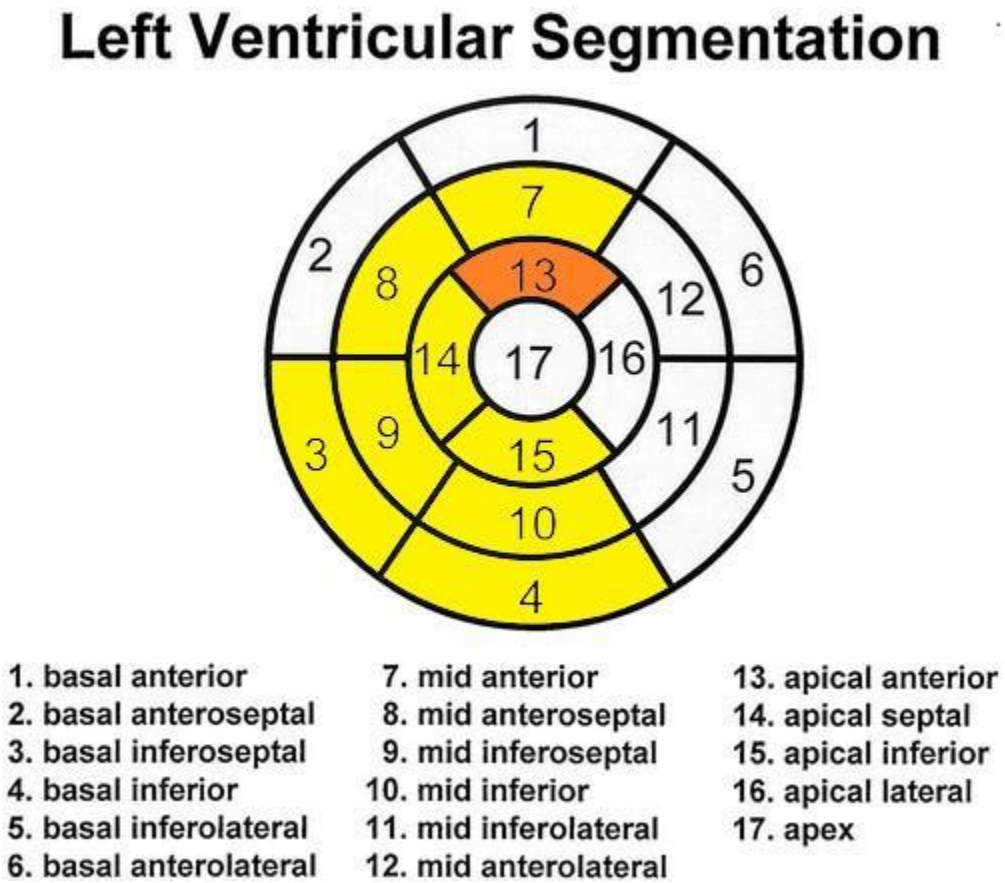

(Figure 3.2) Visualization of co-localization probabilities for left ventricular circumferential strain segments from **(Figure 3.1)** on a 17-section polar chart of the left ventricle.

Male Dataset

The male-only dataset is visible in **(Figure 3.3)**. Fine-mapped association analysis does not show strong associations between *MTSS1* enhancer variants and CMR traits. In particular, associations that were evident in the combined dataset for LVEF, left ventricular circumferential strain, LVESV, and LVEDV are absent. Colocalization analysis between enhancer variants, expression, and CMR traits shows limited to no co-localization for CMR traits such as LVEF, LVESV, LVEDV, or global left ventricular circumferential strain (ColocPR: LVEF = 0.658, LVESV = 0.311, LVEDV = 0.050, Ecc_Global = 0.378). The same lack of colocalization is displayed by left ventricular circumferential strain segments **(Figure 3.4)**.

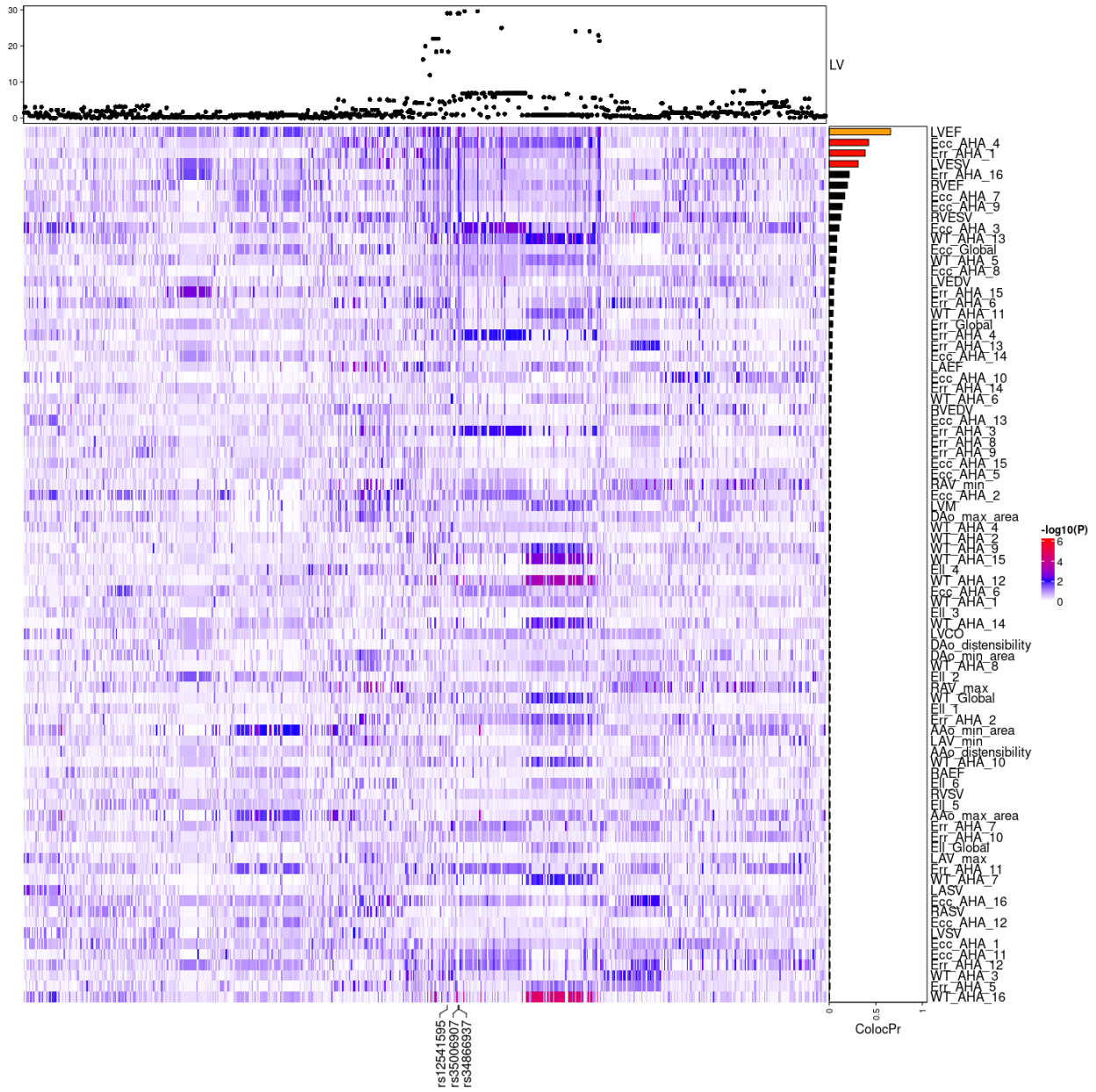

(Figure 3.3) Association of *MTSS1* enhancer variation with CMR traits and colocalization with *MTSS1* expression in GTEx for the male-only dataset.

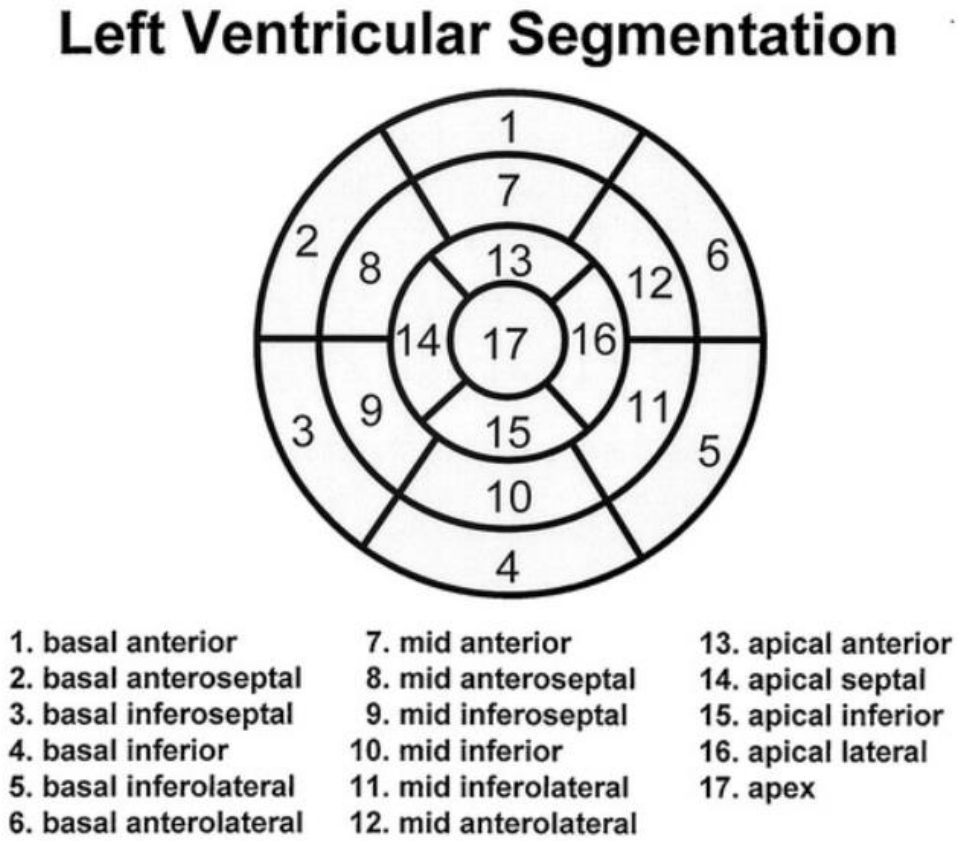

(Figure 3.4) Visualization of co-localization probabilities for left ventricular circumferential strain segments from **(Figure 3.3)** on a 17-section polar chart of the left ventricle.

Female Dataset

Fine-mapping associations between *MTSS1* enhancer variants and CMR traits for biologically female subjects reveals associations between variants and traits such as LVESV, LVEDV, left ventricular global circumferential strain, and LVEF **(Figure 3.5)**. Strong colocalizations exist between *MTSS1* expression, enhancer variants, and CMR traits; *MTSS1* reducing alleles are linked with lower LVESV, higher LVEF, lower left ventricular global circumferential strain, and lower LVEDV (ColocPr: LVESV = 0.991, LVEF = 0.990, Ecc_Global = 0.990, LVEDV = 0.784). For individual left ventricular segments, strong co-localization is detected in mid and apical septal/inferior regions, plus the apical anterior segment **(Figure 3.6)**.

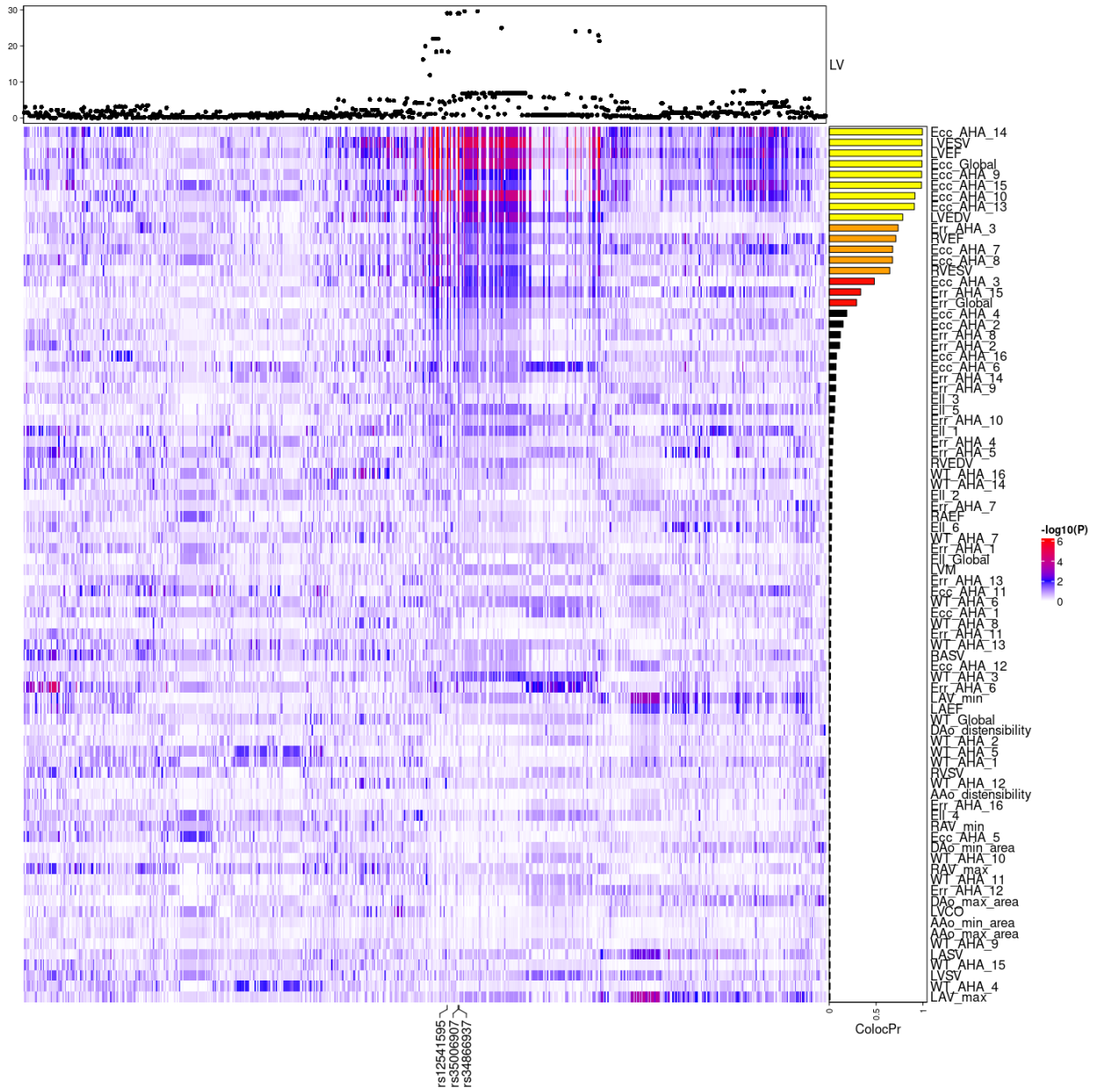

(Figure 3.5) Association of *MTSS1* enhancer variation with CMR traits and colocalization with *MTSS1* expression in GTEx for the female-only dataset.

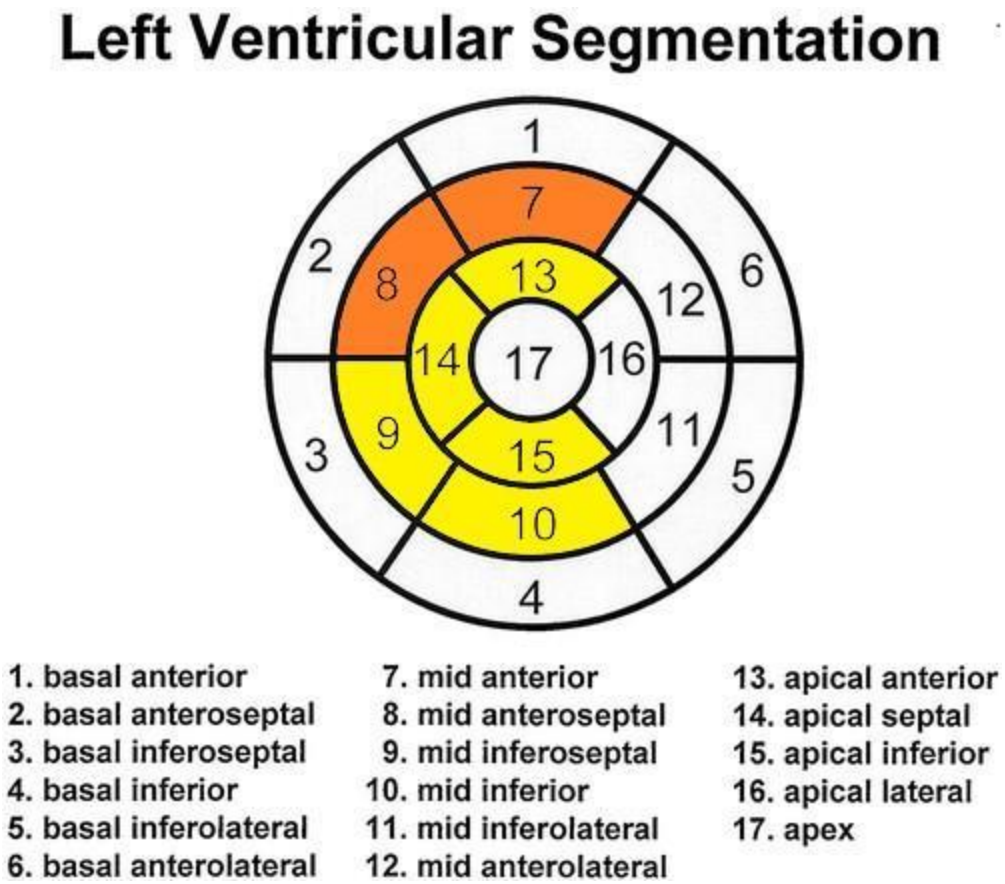

(Figure 3.6) Visualization of co-localization probabilities for left ventricular circumferential strain segments from **(Figure 3.5)** on a 17-section polar chart of the left ventricle.

Chapter 4: MURINE STUDIES

M-mode Echocardiography

Female mice with genetic DCM and global *Mtss1* downregulation exhibit amelioration of their DCM phenotype. Non-transgenic *Mtss1*$^{+/+}$ and *Mtss1*$^{+/-}$ mice show no statistically significant differences in heart rate or left ventricular mass and dimensions quantified via echocardiography **(Figure 4.1, A)**. Consistent with prior published results, *Tg(Myh6-Tpm1*D230N) Mtss1*$^{+/+}$ mice (hereafter referred to as Tg/*Mtss1*$^{+/+}$) show elevated left ventricular mass/mass index, reduced fractional shortening, and increased left ventricular systolic/diastolic dimension relative to their non-pathogenic wild-type (WT)/*Mtss1*$^{+/+}$ counterparts. Tg/*Mtss1*$^{+/-}$ mice demonstrate a statistically significant reduction in left ventricular mass, left ventricular mass index, and left ventricular systolic/diastolic dimension compared with transgenic *Mtss1*$^{+/+}$ mice **(Figure 4.1, B and C)**. Although statistical significance was not reached, a trend towards increased fractional shortening may also exist between the same two groups of mice.

Male mice with DCM, in contrast to their female counterparts, do not appear to be affected by *Mtss1* haploinsufficiency. Similar to their female counterparts, WT/*MTSS1*$^{+/+}$ and WT/*MTSS1*$^{+/-}$ mice have no statistically significant differences in cardiac phenotypes quantified via echocardiography **(Figure 4.1)**. The Tg/*Mtss1*$^{+/+}$ mice show significantly elevated left ventricular mass, mass index, diastolic dimension, and systolic dimension relative to non-transgenic *Mtss1*$^{+/+}$ mice, consistent with prior published results. Unlike the trend observed in female mice, Tg/*Mtss1*$^{+/+}$ and *Mtss1*$^{+/-}$ male mice do not have any significant echocardiographic differences with respect to left ventricular mass, systolic dimension, or diastolic dimension. No trend is apparent for fractional shortening or left ventricular mass index.

A)

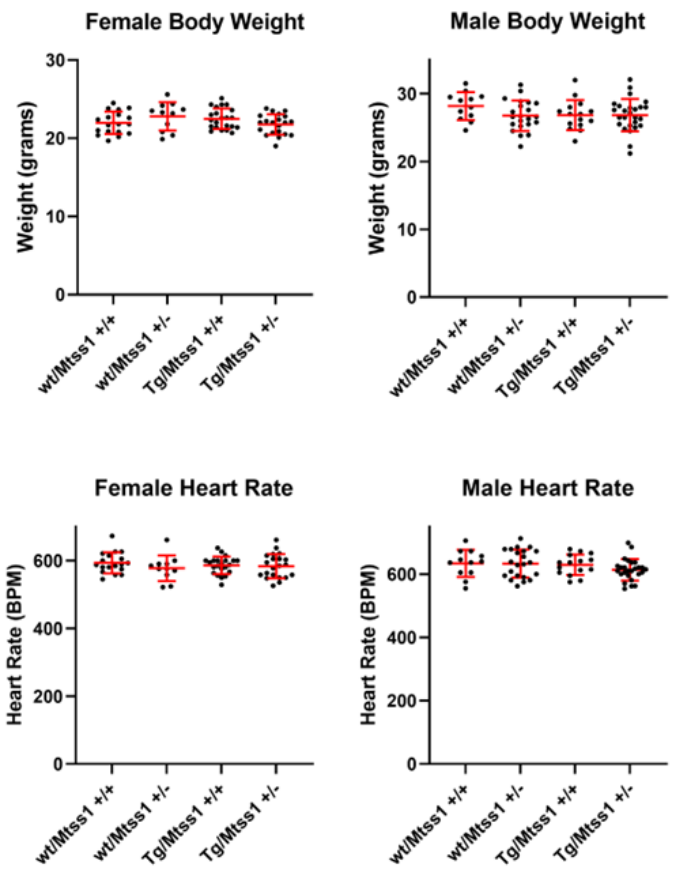
Female Body Weight
Weight (grams)
30
20
10
0
wt/Mtss1 +/+
wt/Mtss1 +/-
Tg/Mtss1 +/+
Tg/Mtss1 +/-
Male Body Weight
Weight (grams)
30
20
10
0
wt/Mtss1 +/+
wt/Mtss1 +/-
Tg/Mtss1 +/+
Tg/Mtss1 +/-
Female Heart Rate
Heart Rate (BPM)
600
400
200
0
wt/Mtss1 +/+
wt/Mtss1 +/-
Tg/Mtss1 +/+
Tg/Mtss1 +/-
Male Heart Rate
Heart Rate (BPM)
600
400
200
0
wt/Mtss1 +/+
wt/Mtss1 +/-
Tg/Mtss1 +/+
Tg/Mtss1 +/-

B)

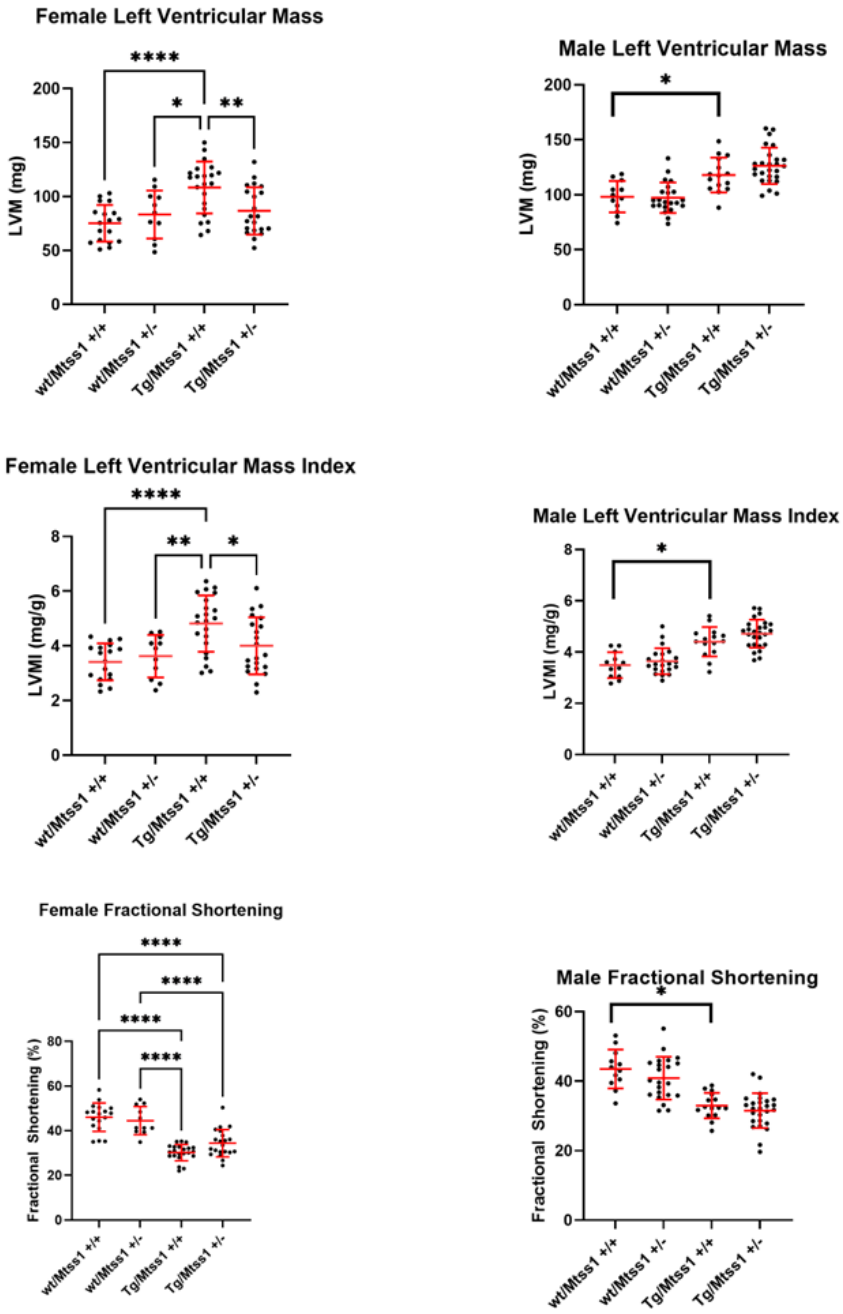
Female Left Ventricular Mass
LVM (mg)
****
*
**
Male Left Ventricular Mass
LVM (mg)
*
Female Left Ventricular Mass Index
LVMI (mg/g)
****
**
*
Male Left Ventricular Mass Index
LVMI (mg/g)
*
Female Fractional Shortening
Fractional Shortening (%)
****
****
****
****
Male Fractional Shortening
Fractional Shortening (%)
*
wt/Mtss1 +/+
wt/Mtss1 +/-
Tg/Mtss1 +/+
Tg/Mtss1 +/-

C)

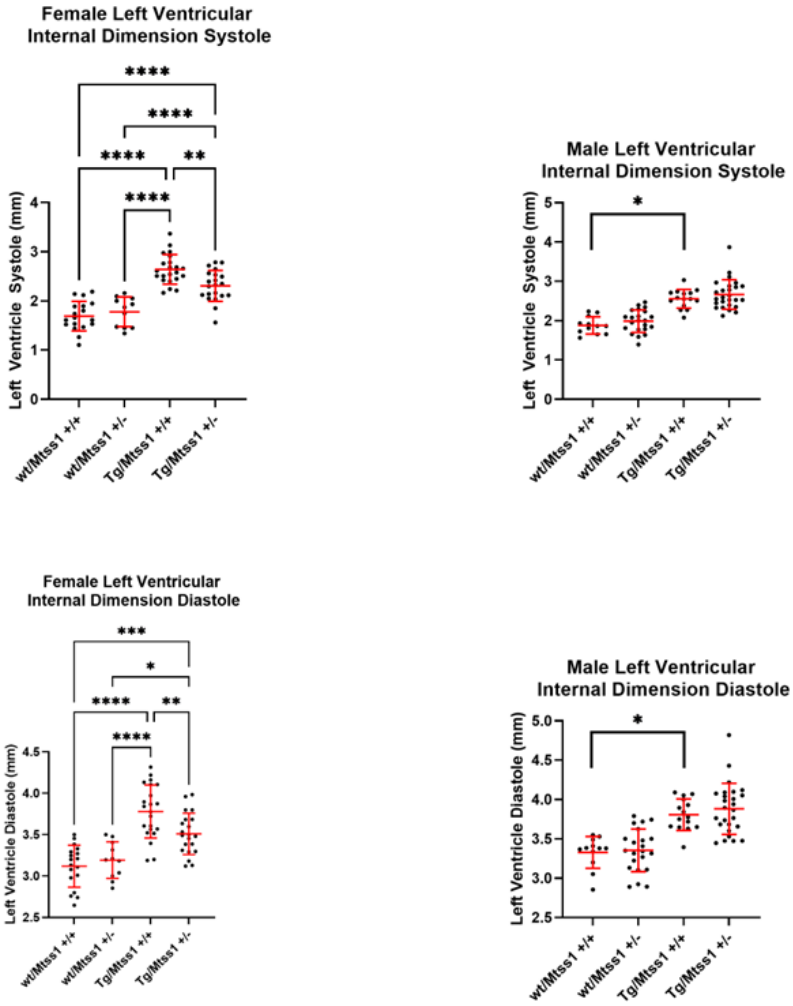
Female Left Ventricular
Internal Dimension Systole
Left Ventricle Systole (mm)
****
****
****
**
****
wt/Mtss1 +/+
wt/Mtss1 +/-
Tg/Mtss1 +/+
Tg/Mtss1 +/-
Male Left Ventricular
Internal Dimension Systole
Left Ventricle Systole (mm)
*
Female Left Ventricular
Internal Dimension Diastole
Left Ventricle Diastole (mm)
***
*
****
**
****
Male Left Ventricular
Internal Dimension Diastole
Left Ventricle Diastole (mm)
*

D)

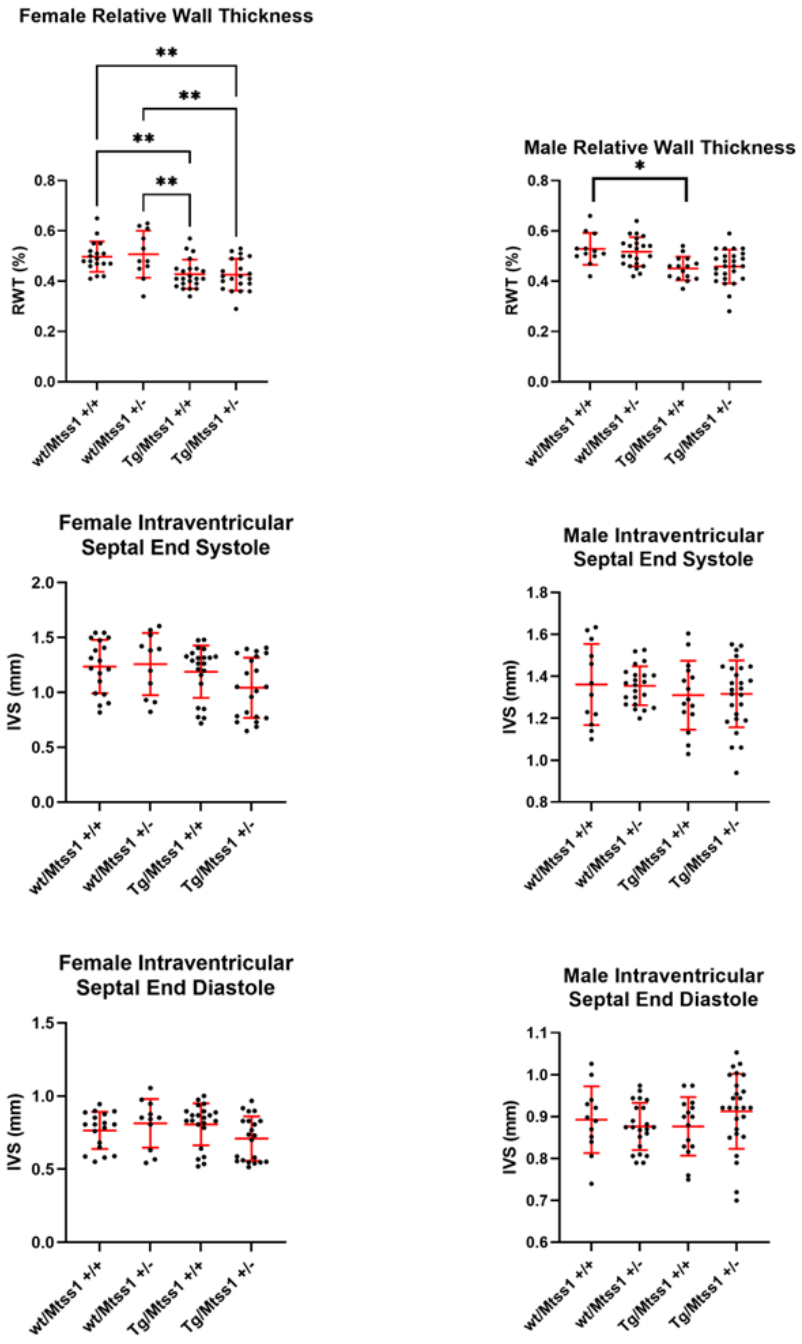
Female Relative Wall Thickness
RWT (%)
Male Relative Wall Thickness
RWT (%)
Female Intraventricular Septal End Systole
IVS (mm)
Male Intraventricular Septal End Systole
IVS (mm)
Female Intraventricular Septal End Diastole
IVS (mm)
Male Intraventricular Septal End Diastole
IVS (mm)
wt/Mtss1 +/+
wt/Mtss1 +/-
Tg/Mtss1 +/+
Tg/Mtss1 +/-

E)

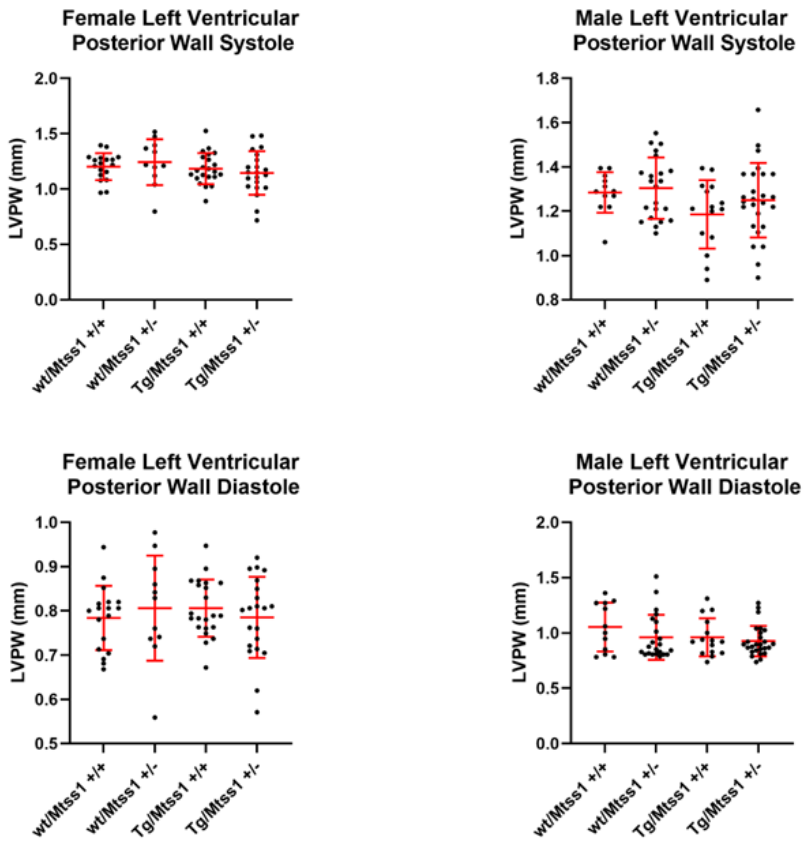

(Figure 4.1) A) Body weight and heart rate of mice. B) Left ventricular mass, left ventricular mass index, and fractional shortening. C) Left ventricular internal dimension systole/diastole. D) Relative wall thickness, intraventricular septal end-systole/diastole. E) Left ventricular posterior wall systole/diastole. Horizontal bars represent mean and standard error. *: P < 0.05, **: P < 0.01, ***: P < 0.001, ****: P <

0.0001. Male mice: wt/*Mtss1* +/+ (12) wt/*Mtss1* +/- (22) Tg/*Mtss1* +/+ (15) Tg/*Mtss1* +/- (26). Female mice: wt/*Mtss1* +/+ (18), wt/*Mtss1* +/- (11), Tg/*Mtss1* +/+ (22), Tg/*Mtss1* +/- (21).

2D Echocardiography

Upon assessment with 2D echocardiographic analysis, female mice exhibit similar cardiac phenotypes across genotypes as those shown with M-mode echocardiography. No group of mice shows significant differences between one another for heart rate or body mass **(Figure 4.2, A)**. Female Tg/*Mtss1*$^{+/+}$ mice show elevated end-systolic and end-diastolic volumes and reduced ejection fraction relative to their wild-type counterparts **(Figure 4.2, B and C)**. Female Tg/*Mtss1*$^{+/-}$ mice show a statistically significant reduction in end-systolic volume and end-diastolic volume compared to Tg/*Mtss1*$^{+/+}$ mice; they also exhibit a significant reduction in ejection fraction (P: EDV = 0.0136, ESV < 0.0001, EF = 0.0005).

Male mice, as observed with M-mode echocardiography, do not show any normalizing effect from *Mtss1* heterozygosity with 2D echocardiography. No significant differences in heart rate or body weight appear to exist across genotypes **(Figure 4.2, A)**. Like their female counterparts, male Tg/*Mtss1*$^{+/+}$ mice demonstrate increased end-systolic and end-diastolic volumes, suggesting left ventricular enlargement. They also exhibit reduced ejection fraction **(Figure 4.2, B and C)**. Unlike in females, male *Mtss1* heterozygosity in the transgenic DCM model does not appear to affect DCM phenotypes such as left ventricular end-systolic volume, end-diastolic volume, or ejection fraction.

A)

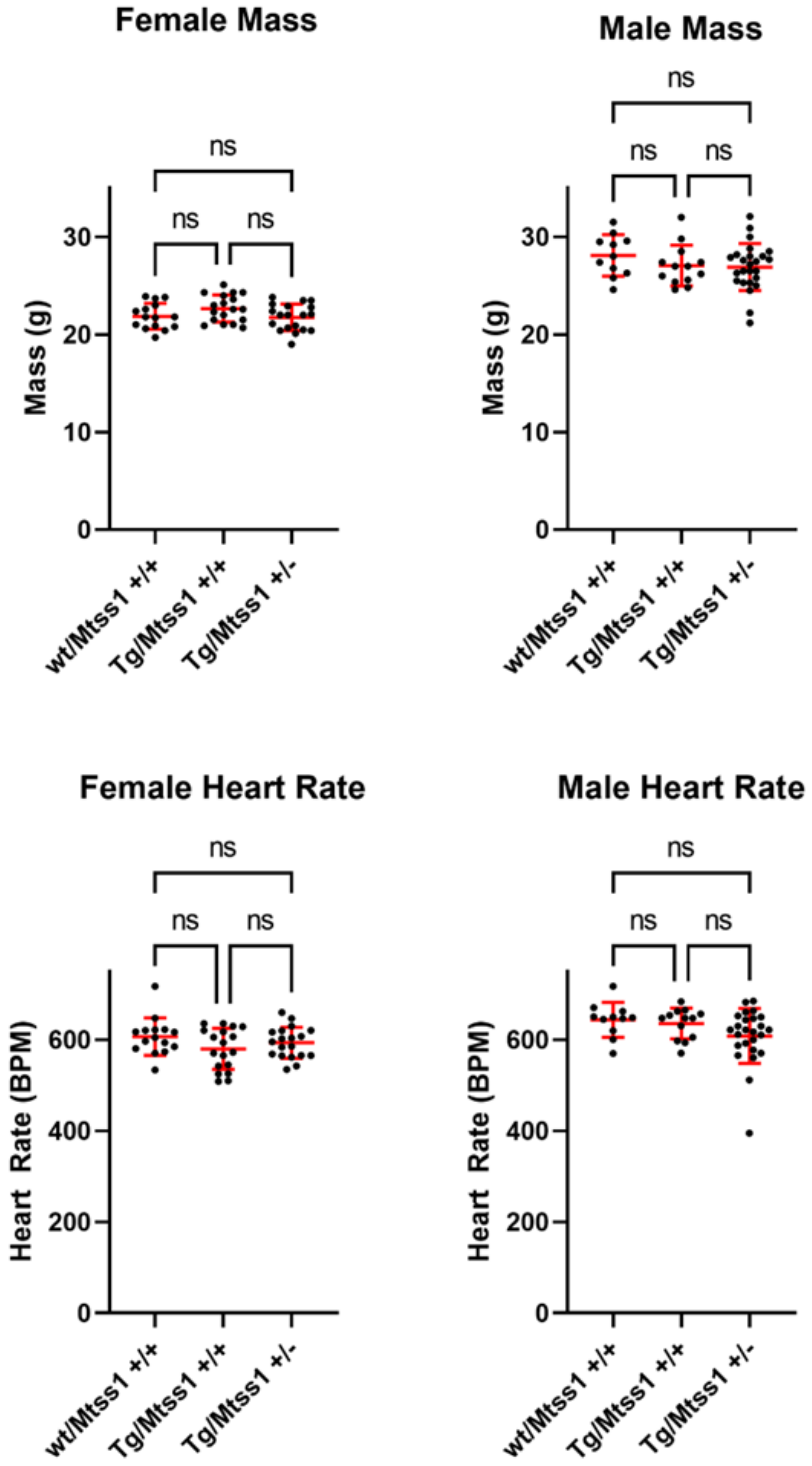
Female Mass
Male Mass
Female Heart Rate
Male Heart Rate
Mass (g)
Heart Rate (BPM)
ns
0
10
20
30
200
400
600
wt/Mtss1 +/+
Tg/Mtss1 +/+
Tg/Mtss1 +/-

B)

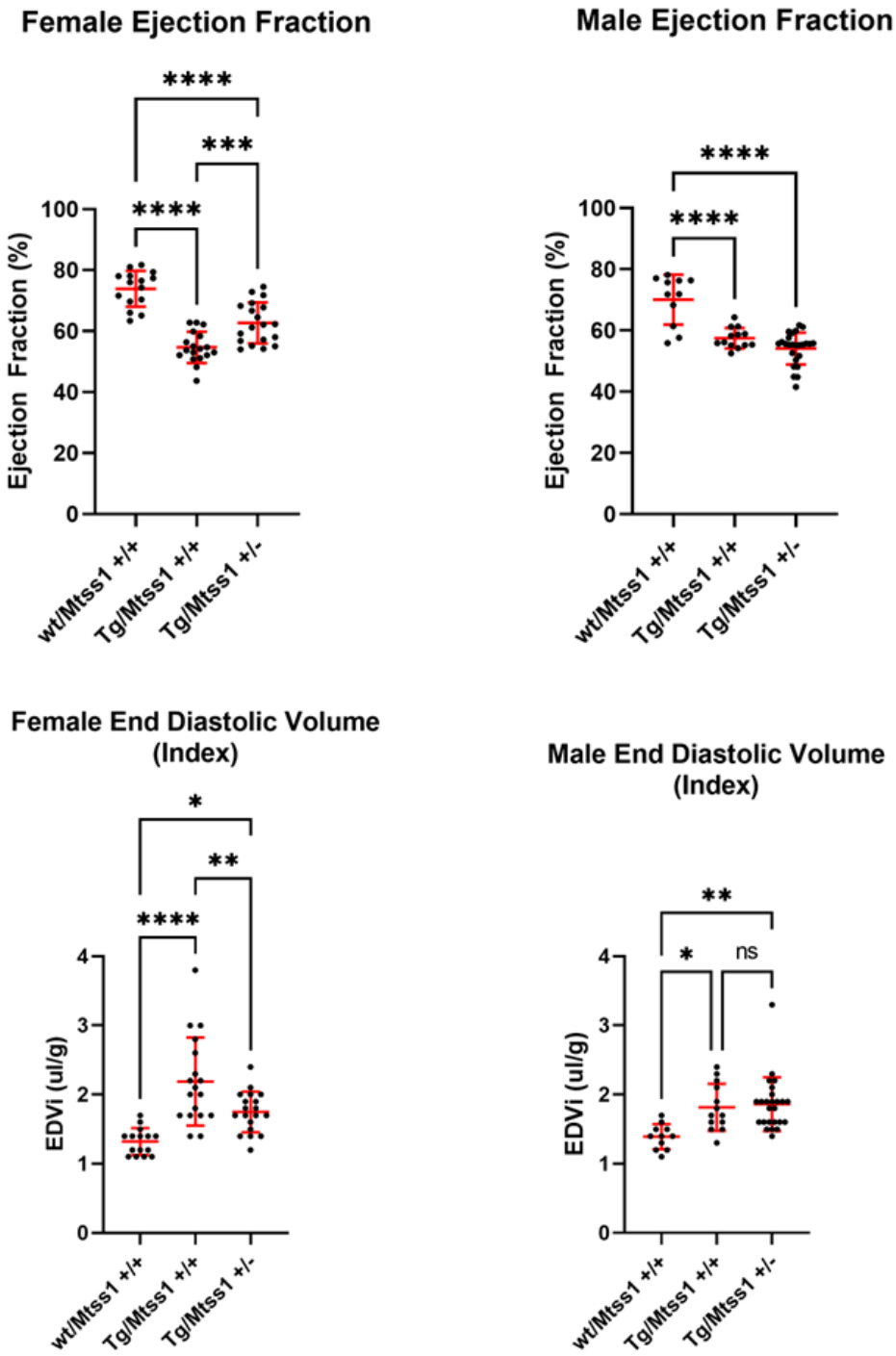
Female Ejection Fraction
Ejection Fraction (%)
100
80
60
40
20
0
****
***
****
wt/Mtss1 +/+
Tg/Mtss1 +/+
Tg/Mtss1 +/-
Male Ejection Fraction
Ejection Fraction (%)
100
80
60
40
20
0
****
****
wt/Mtss1 +/+
Tg/Mtss1 +/+
Tg/Mtss1 +/-
Female End Diastolic Volume (Index)
EDVi (ul/g)
4
3
2
1
0
*
**
****
wt/Mtss1 +/+
Tg/Mtss1 +/+
Tg/Mtss1 +/-
Male End Diastolic Volume (Index)
EDVi (ul/g)
4
3
2
1
0
**
*
ns
wt/Mtss1 +/+
Tg/Mtss1 +/+
Tg/Mtss1 +/-

C)

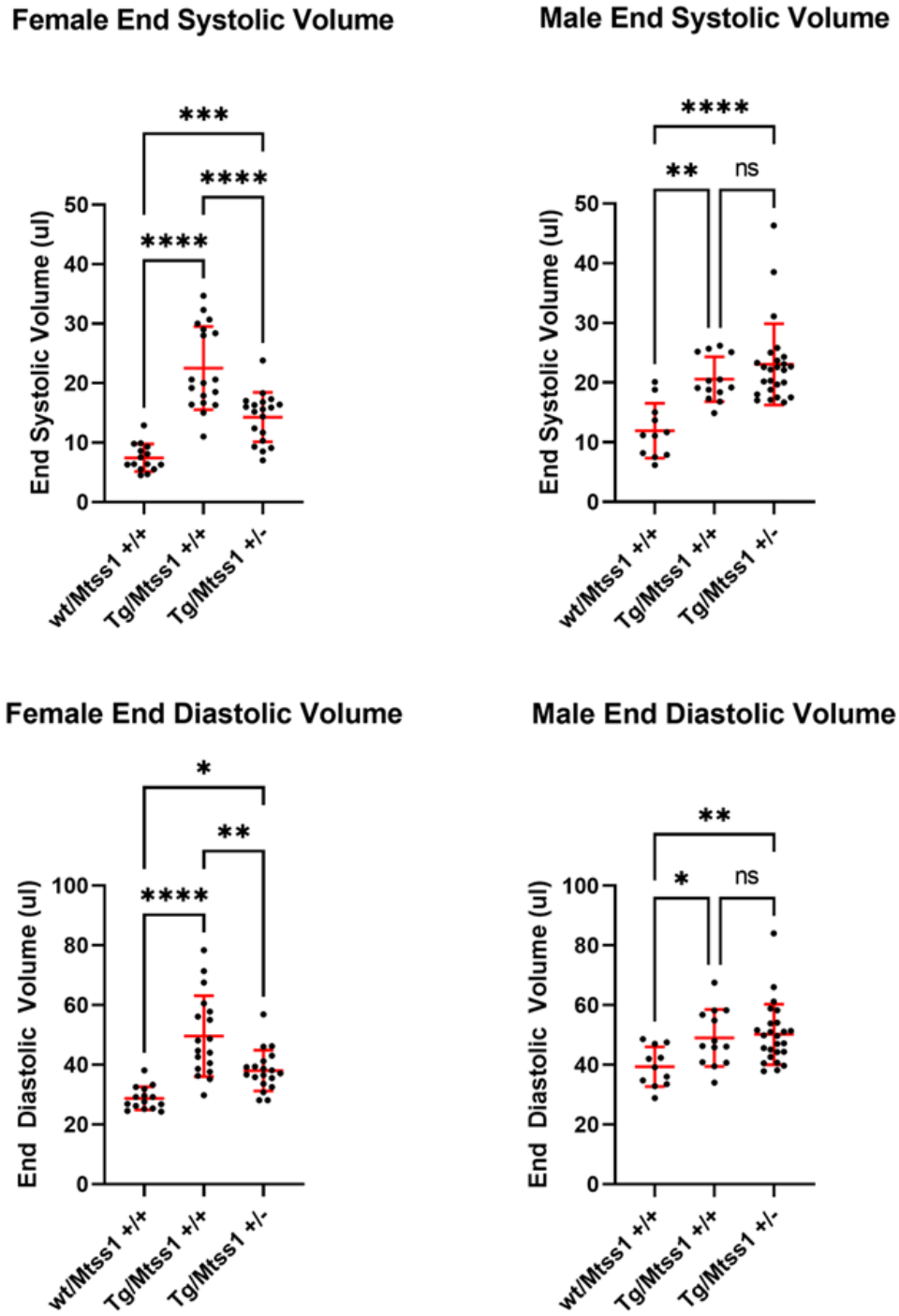
Female End Systolic Volume
End Systolic Volume (ul)
0
10
20
30
40
50
***
****
****
wt/Mtss1 +/+
Tg/Mtss1 +/+
Tg/Mtss1 +/-
Male End Systolic Volume
End Systolic Volume (ul)
0
10
20
30
40
50
****
**
ns
wt/Mtss1 +/+
Tg/Mtss1 +/+
Tg/Mtss1 +/-
Female End Diastolic Volume
End Diastolic Volume (ul)
0
20
40
60
80
100
*
**
****
wt/Mtss1 +/+
Tg/Mtss1 +/+
Tg/Mtss1 +/-
Male End Diastolic Volume
End Diastolic Volume (ul)
0
20
40
60
80
100
**
*
ns
wt/Mtss1 +/+
Tg/Mtss1 +/+
Tg/Mtss1 +/-

(Figure 4.2) A) Body weight and heart rate of mice. B) Ejection fraction and end-diastolic volume (index). C) End-systolic volume and end-diastolic volume. Horizontal bars represent mean and standard error. *: $P < 0.05$, **: $P < 0.01$, ***: $P < 0.001$, ****: $P < 0.0001$. Male mice: wt/*Mtss1* +/+ (11), Tg/*Mtss1* +/+ (13), Tg/*Mtss1* +/- (25). Female mice: wt/*Mtss1* +/+ (15), Tg/*Mtss1* +/+ (18), Tg/*Mtss1* +/- (19).

RNA Sequencing

We did not detect changes in the transcriptomes of murine left ventricular tissue in response to global *Mtss1* heterozygosity in adult mice. A comparison of the transcriptomic profiles between the left ventricular tissues of wild-type mice and heterozygous *Mtss1* knockout mice did not identify any gene that had a statistically significant difference in expression across genotypes **(Figure 4.3)**. Likewise, no notable differences in gene expression were identified in left ventricular tissues harvested from Tg/*Mtss1*$^{+/+}$ and non-transgenic *Mtss1*$^{+/+}$ mice, although *Tpm1* transcript abundance was elevated in Tg mice when compared to non-Tg littermates, as expected. Additionally, we were unable to identify significant differences in sex-stratified analyses **(Figure 4.4, Figure 4.5)**.

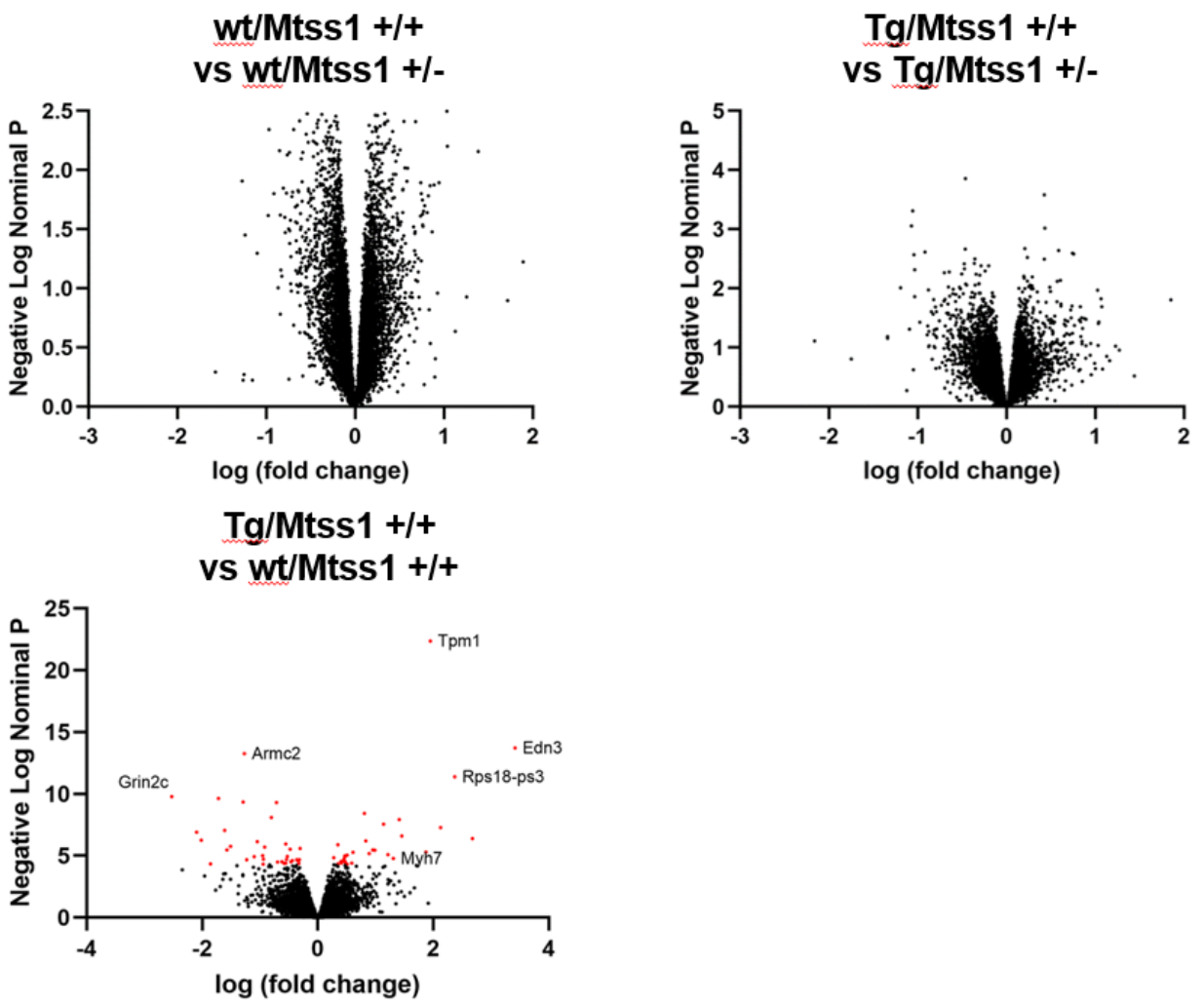

(Figure 4.3) Volcano plots for gene expression changes. The top left plot compares gene expression for wild-type mice (4 male plus 3 female) against *Mtss1* heterozygotes (4 male plus 5 female). The top right plot compares transgenic mice (3 male plus 4 female) against transgenic mice heterozygous for *Mtss1* (5 male plus 4 female). The bottom left plot compares transgenic mice (3 male plus 4 female) against wild-type mice (4 male plus 3 female). Note that these figures display nominal P values on a negative log scale. No changes were statistically significant for either the transgenic or wild-type heterozygous *Mtss1* comparisons after adjusting P values for multiple comparisons.

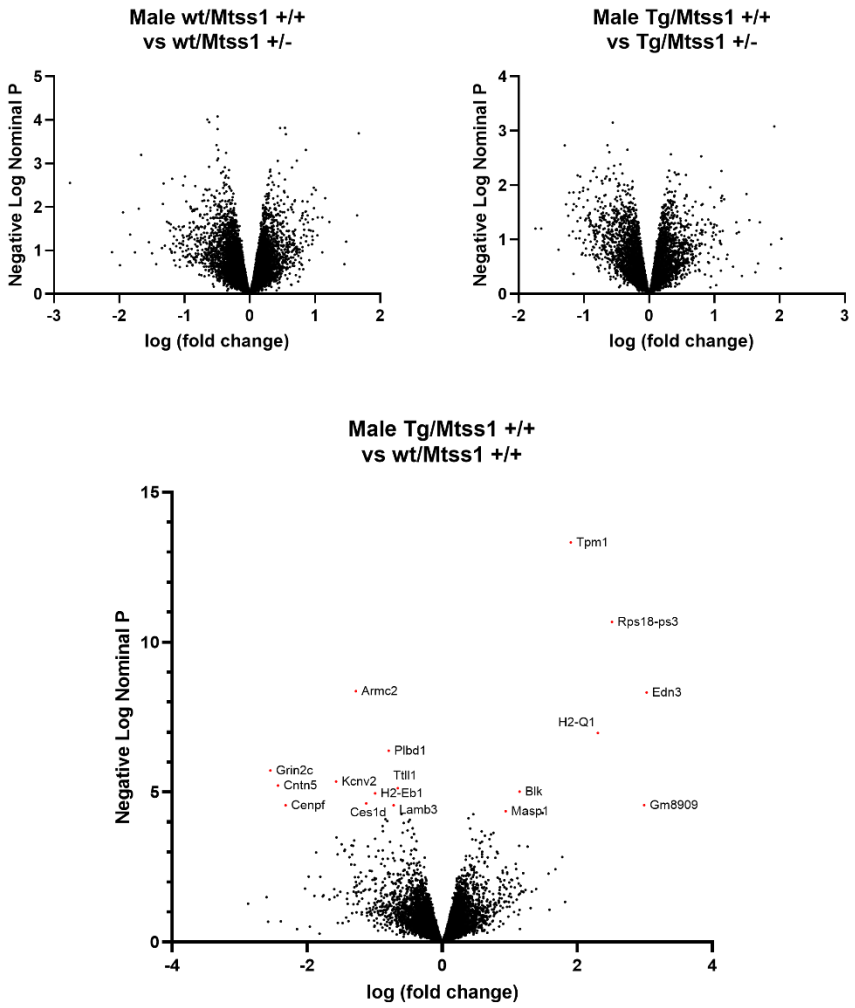

(Figure 4.4) Volcano plots for gene expression changes for male mice only. The top left plot compares gene expression for wild-type mice (4) against *Mtss1* heterozygotes (4). The top right plot compares transgenic mice (3) against transgenic mice heterozygous for *Mtss1* (5). The bottom left plot compares transgenic mice (3) against wild-type mice (4). Note that these figures display nominal P values on a negative log scale. No changes were statistically significant for either the transgenic or wild-type heterozygous *Mtss1* comparisons after adjusting P values for multiple comparisons.

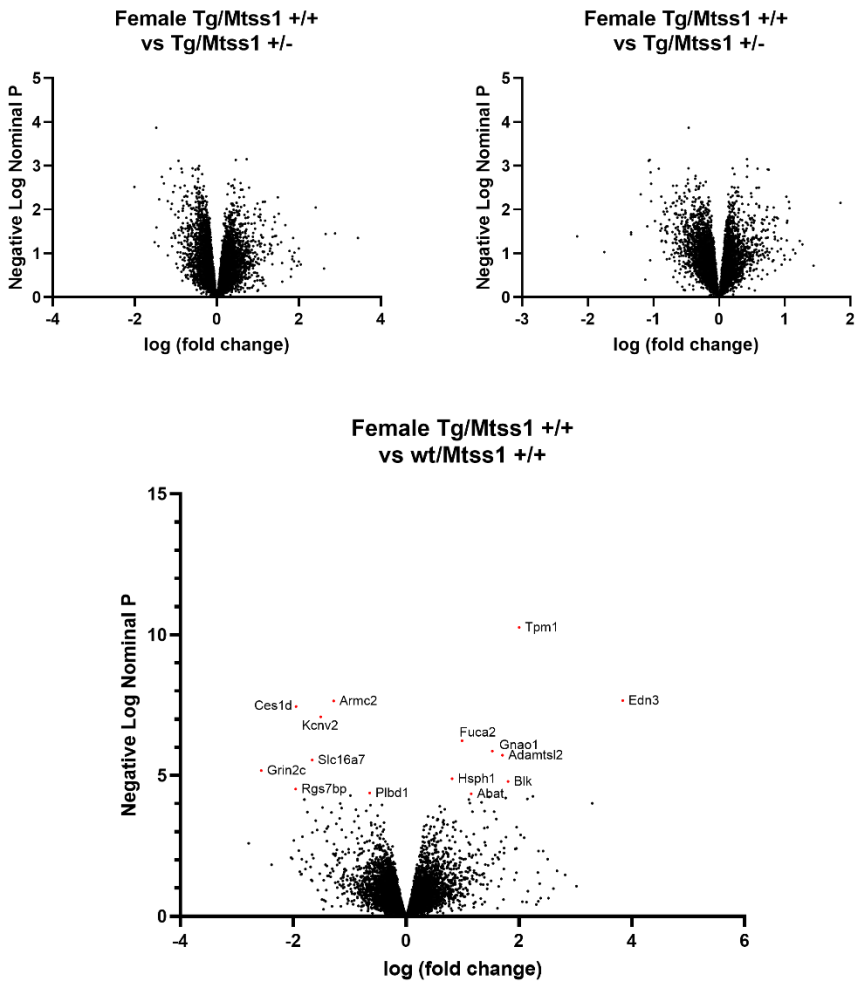

(Figure 4.5) Volcano plots for gene expression changes for female mice only. The top left plot compares gene expression for wild-type mice (3) against *Mtss1* heterozygotes (5). The top right plot compares transgenic mice (4) against transgenic mice heterozygous for *Mtss1* (4). The bottom left plot compares transgenic mice (4) against wild-type mice (3). Note that these figures display nominal P values on a negative log scale. No changes were statistically significant for either the transgenic or wild-type heterozygous *Mtss1* comparisons after adjusting P values for multiple comparisons.

FLAG Immunohistochemistry

High levels of fluorescence were detected in E14.5 embryonic neural tissue between the 3× FLAG C-terminus mice and their wild-type siblings **(Figure 4.6)**. Differences in fluorescence between control and 3× FLAG embryonic cardiac tissue were indeterminate, although there appear to be some signal in the endocardium.

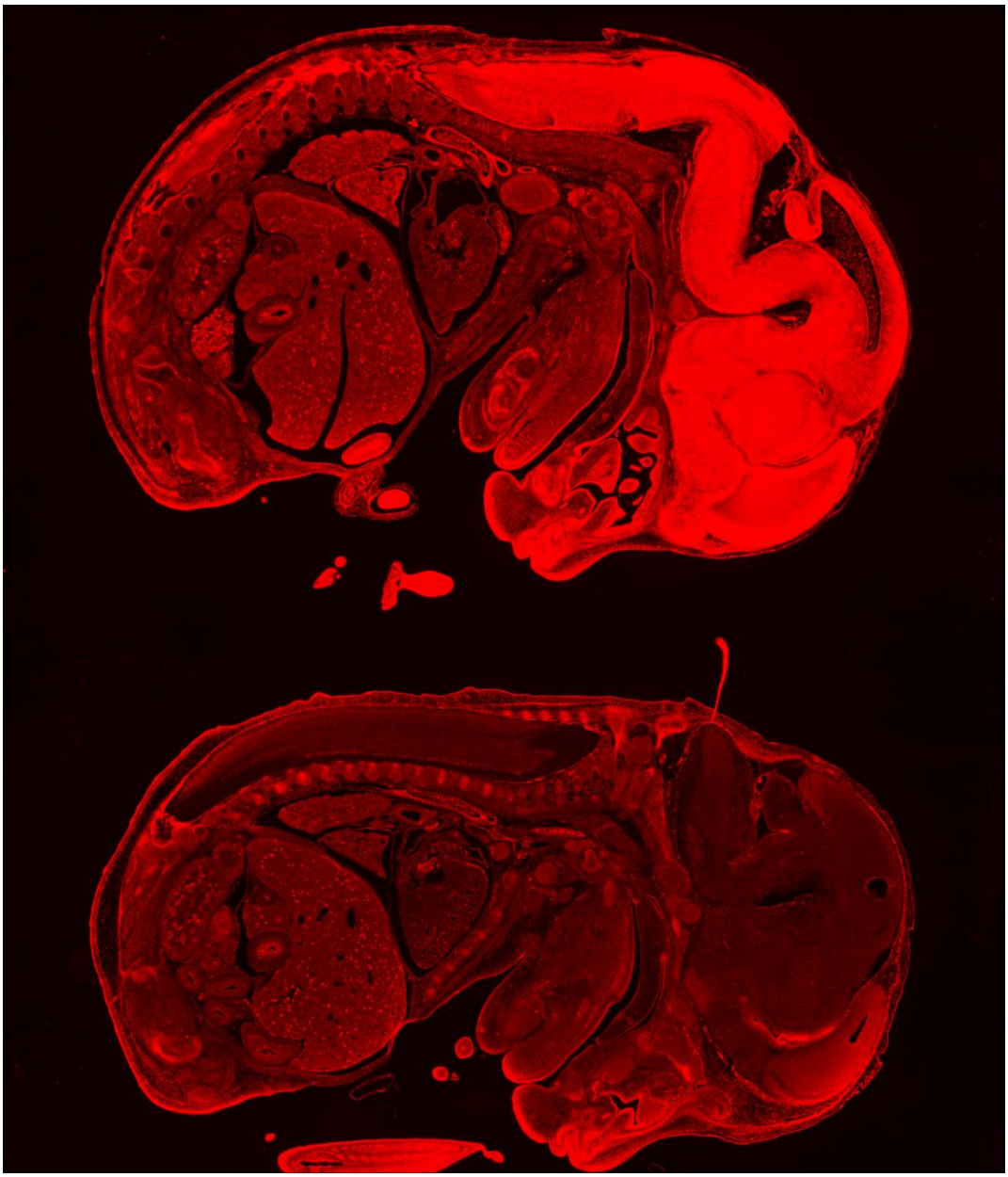

(Figure 4.6) Sagittal section of E14.5 embryos. The top embryo is homozygous for the 3× FLAG C-terminus allele. The bottom embryo is wild-type.

RT-qPCR

We assessed *Tpm1* expression in adult hearts to ensure there was no differential transgene expression by sex. Both wild-type males and females had significantly lower levels of *Tpm1* expression relative to their transgenic counterparts (P < 0.001). Statistical significance was not observed for sex-specific differences in *Tpm1* expression for either wild-type or transgenic mice **(Figure 4.7)**.

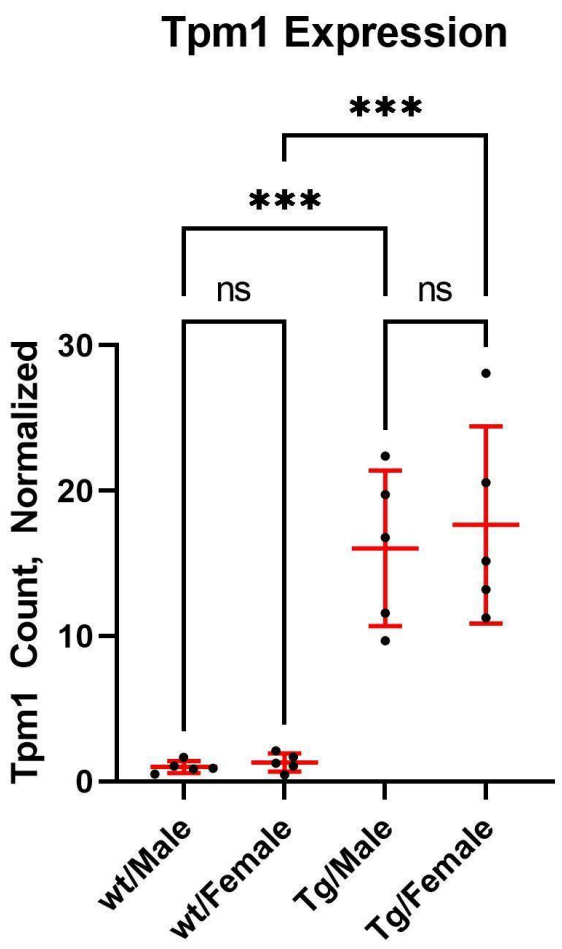

(Figure 4.7) Normalized *Tpm1* count in wild-type and transgenic mice. Normalization was conducted across all genotypes by the division of the raw Tpm1 count by the averaged wild-type male *Tpm1* count. ***: P < 0.001.

Chapter 5: iPSC-CARDIOMYOCYTES

***TNNT2* R173W iPSC-cardiomyocytes**

MTSS1 knockout restores isoproterenol sensitivity to *TNNT2* R173W iPSC-cardiomyocytes. We first introduced the *TNNT2* R173W variant, a known DCM pathogenic variant, into iPSCs from a healthy person (DiPS 1016 SevA, termed 1016, obtained from the Harvard Stem Cell Institute iPS Core Facility), by CRISPR-Cas9-mediated homology-directed repair. Non-pathogenic 1016 iPSC-cardiomyocytes showed an increase in spontaneous beating rate after exposure to the isoproterenol treatment **(Figure 5.1)**. Pathogenic *TNNT2* R173W iPSC-cardiomyocytes showed a statistically significant decrease in spontaneous beating rate relative to their non-pathogenic counterparts (P = 0.001). Then we used CRISPR-Cas9 with two guide RNAs to knock out *MTSS1* via excision of exon 1 and differentiated the cells into cardiomyocytes. iPSC-cardiomyocytes carrying the *TNNT2* R173W mutation and also homozygous for *MTSS1* knockout had a beating rate comparable to that of non-pathogenic iPSC cardiomyocytes.

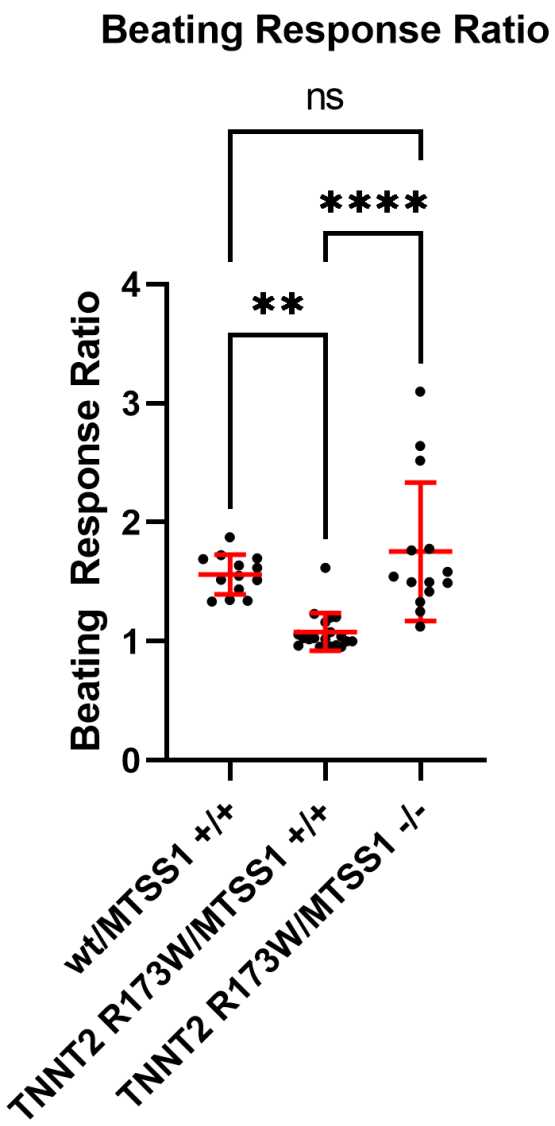

(Figure 5.1) The beating response ratio of iPSC-cardiomyocytes after addition of 1 µM isoproterenol. Beating response ratio is equal to the post-isoproterenol spontaneous beating rate divided by the pre-isoproterenol spontaneous beating rate. Horizontal bars indicate mean and standard error. **: $P < 0.01$, ****: $P < 0.0001$.

***TPM1* D230N iPSC-cardiomyocytes**

TPM1 D230N iPSC-cardiomyocytes did not exhibit isoproterenol insensitivity. Much like our prior experiment with *TNNT2* R173W iPSC-cardiomyocytes, non-pathogenic iPSC-cardiomyocytes showed an increased spontaneous beating rate in response to isoproterenol **(Figure 5.2)**. Unlike *TNNT2* R173W cells, *TPM1* D230N cells increased their spontaneous beating rate with isoproterenol exposure. This increase was statistically indistinguishable from non-pathogenic iPSC cardiomyocytes. *MTSS1* knockout in this model did not cause any detectable change in spontaneous beating rates in either the wild-type or *TPM1* D230N model.

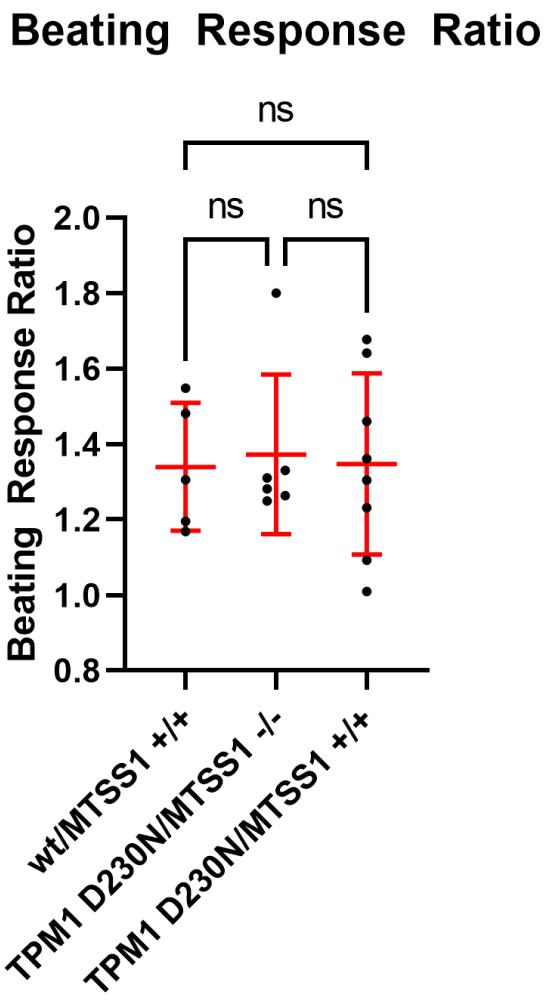

(Figure 5.2) The beating response ratio of iPSC-cardiomyocytes after addition of 1 µM isoproterenol. Beating response ratio is equal to the post-isoproterenol spontaneous beating rate divided by the pre-isoproterenol spontaneous beating rate. Horizontal bars indicate mean and standard error. **: $P < 0.01$, ****: $P < 0.0001$.

CHAPTER 6: DISCUSSION

Our *in vitro* results indicate that MTSS1 reduction may be cardioprotective. Our *TNNT2* R173W iPSC cardiomyocyte line did not respond to isoproterenol exposure, replicating prior published results with this DCM model **(Figure 5.1)**. However, *MTSS1* knockout in the *TNNT2* R173W iPSC-cardiomyocyte model restored the isoproterenol sensitivity to the level that wild-type iPSC-cardiomyocytes possess. This finding supports past work in mice and bioinformatic analyses that also suggested a cardioprotective function for MTSS1 reduction **(Figure 1.7)**.[36]

However, our human genetic studies and animal experiments paint a more nuanced picture; MTSS1 reduction may be preferentially cardioprotective in the female sex. In our transgenic *Tpm1* D230N DCM mouse model, only female transgenic mice with *Mtss1* heterozygosity displayed an intermediate echocardiographic phenotype between those of wild-type and the transgene-only groups for measurements pertaining to DCM (left ventricular ejection fraction, fractional shortening, systolic/diastolic volume, and mass/dimension); male mice did not show this effect. Concordantly, associations between *MTSS1* enhancer variants and CMR traits in the UK Biobank cohort appear to be almost entirely driven by its female population; male associations are absent both before and after colocalization analysis, whereas female associations are robust.

We have yet to identify the mechanism responsible for the effect of MTSS1 on cardiac physiology. Attempts to identify key genes associated with *MTSS1* downregulation via RNAseq did not yield statistically significant targets of note. Sample sizes were small (minimum of 3 per group), which may have limited power to detect changes, and several samples were swapped, though we were able to

reassign them to the correct group by assessing Tpm1 and mtss1 expression via RNAseq and qPCR. While FLAG immunohistochemistry demonstrated high *Mtss1* expression in neural tissue, no noteworthy differences from the wild-type embryo were apparent in cardiac tissue. Nor did our attempt to create a *TPM1* D230N iPSC-cardiomyocyte model succeed; there was no difference in isoproterenol response between the DCM and non-pathogenic iPSC-cardiomyocyte lines.

The biological effect of sex on heart failure and cardiac disease is poorly understood.[49] Historically, women have been underrepresented in both human and experimental models of cardiovascular disease.[50] The sex chromosomes remain understudied in large-scale genetic studies; as of 2021, only 25 percent of the genome-wide summary statistics reported in the NHGRI-EBI GWAS Catalog provide results for the X chromosome, and only three percent provide results for the Y chromosome.[51] Much of this difficulty is due to a few quirks unique to the sex chromosomes themselves. Women have two X chromosomes while men have just one; this lowers the signal associated with male variants in standard array genotyping platforms.[52] X chromosomes commonly undergo random silencing in women; worse, roughly a third of the genes on the X chromosome are expressed on both the silenced and active chromosome (with varying degrees of inactivation escape). X inactivation thereby poses analytical challenges that require X-specific approaches.[53]

To our knowledge, the work in this thesis represents the first time that *MTSS1* has been linked with a cardioprotective effect against genetic dilated cardiomyopathy in a sex-specific manner. This represents a significant addition to prior work concerning the effect of *MTSS1* on dilated cardiomyopathy, as discussed in the Introduction. However, the mechanism of action for the sex-specific cardioprotective

effect remains to be defined. As such, there are multiple different directions in which this work can be taken in the future.

We could deepen our search into the mechanism of effect of MTSS1 on DCM. One possibility is that the primary effect of MTSS1 takes place during development, not in adulthood; the majority of our animal experiments were performed in adult mice. RNAseq on embryonic left ventricular tissue could be of interest for pursuing this line of study. We could also utilize our 3× FLAG C-terminus mouse model; for example, we could section embryos at varying stages of development to track changes in *Mtss1* expression.

It is unclear whether the sex specificity exhibited by MTSS1 vis-à-vis cardioprotection is the result of direct or indirect regulation of activity of MTSS1 by a sex hormone. Ovariectomy of female mice or orchiectomy of male mice could be a next step for testing hypotheses related to sex hormone regulation of MTSS1. If no difference is found, it may be possible that some other factor located on the X or Y chromosome has an effect on MTSS1.

More broadly, the timing of any potential MTSS1 regulation may be of interest. Our qPCR results indicate that MTSS1 mRNA does not appreciably differ in quantity between the sexes; pre-transcriptional regulation is unlikely. However, post-transcriptional and post-translational regulation are both possibilities, with post-translational being more likely. While we were unable to identify other binding partners of MTSS1 via co-immunoprecipitation/pulldown, other assays such as biotinylation identification may yield better results.

An alternative mechanistic possibility is that the effect of MTSS1 is correlated with sex specificity, not caused by it. For example, one possibility is that the action of MTSS1 is linked to body size. As women are smaller than men on average, biological sex could be a correlated variable, not a causative one. Covariate analysis in the UK Biobank or Penn Medicine BioBank may be useful for ruling out these possibilities. Another possibility is that the effect of MTSS1 is driven through action on one of the many cell types that comprise cardiac tissue; it has been previous established that cardiac cellularity is dependent on gonadal hormones.[52] Restricting *Mtss1* expression in cardiomyocytes via a Cre-lox system driven by a cardiomyocyte-specific promoter may be of use for testing this hypothesis.

Instead of focusing narrowly on the mechanism of MTSS1, we could broaden our analyses to better understand the impact of sex on the genetic underpinnings of heart failure. The genetic basis of DCM is diverse.[54] Furthermore, numerous other loci have been implicated in heart failure. However, few of them have been tested for sex-specific effects. Sex-stratified analyses may be able to sort loci associated with DCM into sex-agnostic and sex-specific categories for further examination. Select loci could then be tested in a similar manner as performed with the *MTSS1* locus in this thesis.

BIBLIOGRAPHY

1. Bozkurt B, Coats AJ, Tsutsui H, et al. Universal Definition and Classification of Heart Failure. *J Card Fail*. 2021;27(4):387-413. doi:10.1016/j.cardfail.2021.01.022Cardiac MTSS1 Downregulation

2. Kemp CD, Conte JV. The pathophysiology of heart failure. *Cardiovasc Pathol*. 2012;21(5):365-371. doi:10.1016/j.carpath.2011.11.007

3. Roger VL. Epidemiology of Heart Failure: A Contemporary Perspective. *Circ Res*. 2021;128(10):1421-1434. doi:10.1161/CIRCRESAHA.121.318172

4. Savarese G, Becher PM, Lund LH, Seferovic P, Rosano GMC, Coats AJS. Global burden of heart failure: a comprehensive and updated review of epidemiology. *Cardiovasc Res*. 2023;118(17):3272-3287. doi:10.1093/cvr/cvac013

5. Heidenreich PA, Albert NM, Allen LA, et al. Forecasting the Impact of Heart Failure in the United States: A Policy Statement From the American Heart Association. *Circ Heart Fail*. 2013;6(3):606-619. doi:10.1161/HHF.0b013e318291329a

6. Fedele M, Piersanti R, Regazzoni F, et al. A comprehensive and biophysically detailed computational model of the whole human heart electromechanics. *Comput Methods Appl Mech Eng*. 2023;410:115983. doi:10.1016/j.cma.2023.115983

7. Olshansky B, Ricci F, Fedorowski A. Importance of resting heart rate. *Trends Cardiovasc Med*. 2023;33(8):502-515. doi:10.1016/j.tcm.2022.05.006

8. Ho D, Zhao X, Gao S, Hong C, Vatner DE, Vatner SF. Heart Rate and Electrocardiography Monitoring in Mice. *Curr Protoc Mouse Biol*. 2011;1(1):123-139. doi:10.1002/9780470942390.mo100159

9. Maceira A, Prasad S, Khan M, Pennell D. Normalized Left Ventricular Systolic and Diastolic

Function by Steady State Free Precession Cardiovascular Magnetic Resonance. *J Cardiovasc Magn Reson*. 2006;8(3):417-426. doi:10.1080/10976640600572889

10. Kovalova S, Necas J, Cerbak R, Malik P, Vespalec J. Echocardiographic volumetry of the right ventricle. *Eur J Echocardiogr*. 2005;6(1):15-23. doi:10.1016/j.euje.2004.04.009

11. Marwick TH. Ejection Fraction Pros and Cons. *J Am Coll Cardiol*. 2018;72(19):2360-2379. doi:10.1016/j.jacc.2018.08.2162

12. Foley TA, Radiologist, Department of Radiology, Mankad SV, et al. Measuring Left Ventricular Ejection Fraction – Techniques and Potential Pitfalls. *Eur Cardiol Rev*. 2012;8(2):108. doi:10.15420/ecr.2012.8.2.108

13. Kosaraju A, Goyal A, Grigorova Y, Makaryus AN. Left Ventricular Ejection Fraction. In: *StatPearls*. StatPearls Publishing; 2023. Accessed January 15, 2024. http://www.ncbi.nlm.nih.gov/books/NBK459131/

14. Murphy SP, Ibrahim NE, Januzzi JL. Heart Failure With Reduced Ejection Fraction: A Review. *JAMA*. 2020;324(5):488. doi:10.1001/jama.2020.10262

15. Simmonds SJ, Cuijpers I, Heymans S, Jones EAV. Cellular and Molecular Differences between HFpEF and HFrEF: A Step Ahead in an Improved Pathological Understanding. *Cells*. 2020;9(1):242. doi:10.3390/cells9010242

16. Brady B, King G, Murphy RT, Walsh D. Myocardial strain: a clinical review. *Ir J Med Sci*. 2023;192(4):1649-1656. doi:10.1007/s11845-022-03210-8

17. Johnson C, Kuyt K, Oxborough D, Stout M. Practical tips and tricks in measuring strain, strain rate and twist for the left and right ventricles. *Echo Res Pract*. 2019;6(3):R87-R98. doi:10.1530/ERP-19-0020

18. Pu C, Fei J, Lv S, et al. Global Circumferential Strain by Cardiac Magnetic Resonance Tissue

Tracking Associated With Ventricular Arrhythmias in Hypertrophic Cardiomyopathy Patients. *Front Cardiovasc Med*. 2021;8:670361. doi:10.3389/fcvm.2021.670361

19. Reichart D, Magnussen C, Zeller T, Blankenberg S. Dilated cardiomyopathy: from epidemiologic to genetic phenotypes: A translational review of current literature. *J Intern Med*. 2019;286(4):362-372. doi:10.1111/joim.12944

20. Rosenbaum AN, Agre KE, Pereira NL. Genetics of dilated cardiomyopathy: practical implications for heart failure management. *Nat Rev Cardiol*. 2020;17(5):286-297. doi:10.1038/s41569-019-0284-0

21. Fairweather D, Cooper LT, Blauwet LA. Sex and Gender Differences in Myocarditis and Dilated Cardiomyopathy. *Curr Probl Cardiol*. 2013;38(1):7-46. doi:10.1016/j.cpcardiol.2012.07.003

22. Schultheiss HP, Fairweather D, Caforio ALP, et al. Dilated cardiomyopathy. *Nat Rev Dis Primer*. 2019;5(1):32. doi:10.1038/s41572-019-0084-1

23. Pio Loco Detto Gava C, Merlo M, Paldino A, et al. New perspectives in diagnosis and risk stratification of non-ischaemic dilated cardiomyopathy. *Eur Heart J Suppl*. 2023;25(Supplement_C):C137-C143. doi:10.1093/eurheartjsupp/suad016

24. Xu Y, Li W, Wan K, et al. Myocardial Tissue Reverse Remodeling After Guideline-Directed Medical Therapy in Idiopathic Dilated Cardiomyopathy. *Circ Heart Fail*. 2021;14(1):e007944. doi:10.1161/CIRCHEARTFAILURE.120.007944

25. Merlo M, Caiffa T, Gobbo M, Adamo L, Sinagra G. Reverse remodeling in Dilated Cardiomyopathy: Insights and future perspectives. *Int J Cardiol Heart Vasc*. 2018;18:52-57. doi:10.1016/j.ijcha.2018.02.005

26. Simonson MA. Genome-Wide Association Study (GWAS). In: Gellman MD, ed. *Encyclopedia of Behavioral Medicine*. Springer International Publishing; 2020:936-939. doi:10.1007/978-3-030-

39903-0_697

27. Uffelmann E, Huang QQ, Munung NS, et al. Genome-wide association studies. *Nat Rev Methods Primer*. 2021;1(1):59. doi:10.1038/s43586-021-00056-9

28. Frayling TM, Timpson NJ, Weedon MN, et al. A Common Variant in the *FTO* Gene Is Associated with Body Mass Index and Predisposes to Childhood and Adult Obesity. *Science*. 2007;316(5826):889-894. doi:10.1126/science.1141634

29. Siminovitch KA. PTPN22 and autoimmune disease. *Nat Genet*. 2004;36(12):1248-1249. doi:10.1038/ng1204-1248

30. Korte A, Farlow A. The advantages and limitations of trait analysis with GWAS: a review. *Plant Methods*. 2013;9(1):29. doi:10.1186/1746-4811-9-29

31. Slatkin M. Linkage disequilibrium — understanding the evolutionary past and mapping the medical future. *Nat Rev Genet*. 2008;9(6):477-485. doi:10.1038/nrg2361

32. Hormozdiari F, van de Bunt M, Segrè AV, et al. Colocalization of GWAS and eQTL Signals Detects Target Genes. *Am J Hum Genet*. 2016;99(6):1245-1260. doi:10.1016/j.ajhg.2016.10.003

33. Wild PS, Felix JF, Schillert A, et al. Large-scale genome-wide analysis identifies genetic variants associated with cardiac structure and function. *J Clin Invest*. 2017;127(5):1798-1812. doi:10.1172/JCI84840

34. Shah S, Henry A, Roselli C, et al. Genome-wide association and Mendelian randomisation analysis provide insights into the pathogenesis of heart failure. *Nat Commun*. 2020;11(1):163. doi:10.1038/s41467-019-13690-5

35. Levin MG, Tsao NL, Singhal P, et al. Genome-wide association and multi-trait analyses characterize the common genetic architecture of heart failure. *Nat Commun*. 2022;13(1):6914. doi:10.1038/s41467-022-34216-6

36. Morley MP, Wang X, Hu R, et al. Cardioprotective effects of MTSS1 enhancer variants. *Circulation*. 2019;139(17):2073-2076. doi:10.1161/CIRCULATIONAHA.118.037939

37. Lonsdale J, Thomas J, Salvatore M, et al. The Genotype-Tissue Expression (GTEx) project. *Nat Genet*. 2013;45(6):580-585. doi:10.1038/ng.2653

38. Du P, Wang S, Tang X, An C, Yang Y, Jiang WG. Reduced Expression of Metastasis Suppressor-1 (MTSS1) Accelerates Progression of Human Bladder Uroepithelium Cell Carcinoma. *Anticancer Res*. 2017;37(8):4499-4505. doi:10.21873/anticanres.11846

39. Vadakekolathu J, Al-Juboori SIK, Johnson C, et al. MTSS1 and SCAMP1 cooperate to prevent invasion in breast cancer. *Cell Death Dis*. 2018;9(3):344. doi:10.1038/s41419-018-0364-9

40. Zhong J, Shaik S, Wan L, et al. SCFβ-TRCP targets MTSS1 for ubiquitination-mediated destruction to regulate cancer cell proliferation and migration. *Oncotarget*. 2013;4(12):2339-2353.

41. Petrov P, Sarapulov AV, Eöry L, et al. Computational analysis of the evolutionarily conserved Missing In Metastasis/Metastasis Suppressor 1 gene predicts novel interactions, regulatory regions and transcriptional control. *Sci Rep*. 2019;9(1):4155. doi:10.1038/s41598-019-40697-1

42. Parr C, Jiang WG. Metastasis suppressor 1 (MTSS1) demonstrates prognostic value and anti-metastatic properties in breast cancer. *Eur J Cancer*. 2009;45(9):1673-1683. doi:10.1016/j.ejca.2009.02.019

43. Oliva M, Muñoz-Aguirre M, Kim-Hellmuth S, et al. The impact of sex on gene expression across human tissues. *Science*. 2020;369(6509):eaba3066. doi:10.1126/science.aba3066

44. Lynn ML, Tal Grinspan L, Holeman TA, Jimenez J, Strom J, Tardiff JC. The structural basis of alpha-tropomyosin linked (Asp230Asn) familial dilated cardiomyopathy. *J Mol Cell Cardiol*. 2017;108:127-137. doi:10.1016/j.yjmcc.2017.06.001

45. Sun N, Yazawa M, Liu J, et al. Patient-specific induced pluripotent stem cells as a model for

familial dilated cardiomyopathy. *Sci Transl Med*. 2012;4(130):130ra47. doi:10.1126/scitranslmed.3003552

46. Lv W, Qiao L, Petrenko N, et al. Functional Annotation of TNNT2 Variants of Uncertain Significance With Genome-Edited Cardiomyocytes. *Circulation*. 2018;138(24):2852-2854. doi:10.1161/CIRCULATIONAHA.118.035028

47. Veres A, Gosis BS, Ding Q, et al. Low Incidence of Off-Target Mutations in Individual CRISPR-Cas9 and TALEN Targeted Human Stem Cell Clones Detected by Whole-Genome Sequencing. *Cell Stem Cell*. 2014;15(1):27-30. doi:10.1016/j.stem.2014.04.020

48. Palpant NJ, Pabon L, Friedman CE, et al. Generating high-purity cardiac and endothelial derivatives from patterned mesoderm using human pluripotent stem cells. *Nat Protoc*. 2017;12(1):15-31. doi:10.1038/nprot.2016.153

49. Regitz-Zagrosek V, Gebhard C. Gender medicine: effects of sex and gender on cardiovascular disease manifestation and outcomes. *Nat Rev Cardiol*. 2023;20(4):236-247. doi:10.1038/s41569-022-00797-4

50. Reue K, Wiese CB. Illuminating the Mechanisms Underlying Sex Differences in Cardiovascular Disease. *Circ Res*. 2022;130(12):1747-1762. doi:10.1161/CIRCRESAHA.122.320259

51. Sun L, Wang Z, Lu T, Manolio TA, Paterson AD. eXclusionarY: 10 years later, where are the sex chromosomes in GWASs? *Am J Hum Genet*. 2023;110(6):903-912. doi:10.1016/j.ajhg.2023.04.009

52. Squiers GT, McLellan MA, Ilinykh A, Branca J, Rosenthal NA, Pinto AR. Cardiac cellularity is dependent upon biological sex and is regulated by gonadal hormones. *Cardiovasc Res*. 2021;117(10):2252-2262. doi:10.1093/cvr/cvaa265

53. Chen B, Craiu RV, Strug LJ, Sun L. The X factor: A robust and powerful approach to X-chromosome-inclusive whole-genome association studies. *Genet Epidemiol*. 2021;45(7):694-709.

doi:10.1002/gepi.22422

54. Kim KH, Pereira NL. Genetics of Cardiomyopathy: Clinical and Mechanistic Implications for Heart Failure. *Korean Circ J*. 2021 Oct;51(10):797-836. doi: 10.4070/kcj.2021.0154.